Supporting information

Assessment of degradation by-products and NDMA formation potential during UV and UV/H_2O_2 treatment of doxylamine in the presence of monochloramine

Maria José Farré, Jelena Radjenovic*, Wolfgang Gernjak*

Advanced Water Management Centre, The University of Queensland, Queensland 4072, Australia.

The two corresponding authors contributed equally to this work.

*corresponding author 1
Dr Maria José Farré
Phone: +61 7 3346 3233,
Fax: +61 7 3365 4726,
e-mail: m.farre@awmc.uq.edu.au

*corresponding author 2
Dr Jelena Radjenovic
Phone: +61 7 3346 3234,
Fax: +61 7 3365 4726,
e-mail: j.radjenovic@awmc.uq.edu.au

Text S1

NDMA formation potential test and NDMA analysis

A concentration of 2 mM (142 mg/L Cl_2) NH_2Cl was used to determine the NDMA formation potential, in order to ensure that all potential precursors reacted with NH_2Cl to generate NDMA. The test was performed in the dark at pH 6.8 at 23±2^oC. After seven days, the residual chloramine concentration was quenched with 2.5 g/L of sodium sulfite to prevent further NDMA formation. Each NDMA formation potential test was conducted in duplicate, and the results are expressed as mean values with a range.

NDMA samples were directly injected and analyzed by reversed phase high performance liquid chromatography equipped with a photodiode array detector (HPLC-DAD consisting of Shimadzu LC-20 AT Prominence LC, SIL-20A HT Prominence auto sampler and SPD-M20 A Prominence diode array detector). Isocratic elution of NDMA was performed on a 10 cm LiChrosphere RP-select B (Merck, U.S.A) column with 5 um pore size, using 1 mL/min flow with 5% methanol and 95% 10 mM acetate solution buffered at pH 4 as eluent. The limit of detection was 1 µg/L and the analytical method showed linearity up to 1000 µg/L. The peak purity function of the LC solution software supplied by Shimadzu was used to verify the purity of all observed NDMA peaks.

UVC and AOP experiments

During each experiment, 1 mL samples were withdrawn at 0 min, 5 min (250 mJ/cm^2), 15 min (750 mJ/cm^2), 25 min (1250 mJ/cm^2) and 45 min (2250 mJ/cm^2) and immediately frozen in amber glass 2 mL vials for later injection into the QqLIT-MS for the identification of oxidation by-products. Additionally, 50 mL were withdrawn at the same times to immediately perform NDMA formation potential tests. To avoid changes in the volume higher than 10%, two different experiments were performed to obtain the volume required for four NDMA formation potential tests. A third experiment was run to measure complementary experimental data such as chlorine, ammonia, nitrate and hydrogen peroxide.

We are aware that withdrawing samples during the experiment and thereby changing the total liquid volume in the reactor, as well as small changes in UV transmissivity during the experiment will alter the volume averaged irradiance slightly during the experiment affecting the determination of UV dose in comparison to the uridine actinometry. However, it shall be noted that the purpose of the study is not to evaluate the precise UV dose at which the

changes to the NDMA formation potential occur, but rather to prove the general concept that oxidation treatments can increase and decrease NDMA formation potential. The measurement of UV dose is meant to complement the findings to indicate in which UV dose range such changes can be expected to occur.

Free chlorine, total chlorine and hydrogen peroxide were measured during the experiment. Commercial DPD test kits (Hach, U.S.A.) were used for the analysis of free and total chlorine. The hydrogen peroxide concentration was determined spectrophotometrically as described by Nogueira and co-authors [1]. The TOC was measured with an Analytik Jena multi N/C 3100 instrument. For each sample, 2–3 replicates were measured, until a relative standard deviation of less than 3% was obtained. Ammonia and nitrite were measured on a Lachat flow injection analyzer as per the Lachat QuickChem method 31-107-06-1-A. To exclude sources of contamination all experiments were accompanied by blanks measuring the NDMA formation potential of MilliQ water used to prepare the DOX solution. In all cases, the concentration of NDMA formed was below the detection limit. To exclude any contamination from the UVC reactor initial solutions of DOX were recirculated through the reactor before measuring the NDMA formation potential. This reactor blank was also compared to blank of the solution before being fed to the reactor. No significant difference was observed between blank and reactor blank (see also Figure 1 in the main text).

NDMA was not measured during the experiments as its formation from the reaction of DOX by-products with monochloramine is not expected. The direct formation of NDMA from DOX and its by-products would require their reaction with dichloramine, which was not present in the experiments due to a very low rate of monochloramine disproportionation to dichloramine [2], which stands in contrast to the short experiment times in the order of minutes. Furthermore, NDMA is photo labile and exhibits two absorption bands, with one maximum at 228 nm (molar extinction coefficient ε_{228nm}= 7378 $M^{-1}cm^{-1}$) and one at 332 nm (ε_{332nm}=109 $M^{-1}cm^{-1}$) and therefore NDMA formed directly in the experiment would simultaneously be degraded to a large degree [3].

Text S2

The analyses in positive electrospray ionization ((+)ESI) were performed using acetonitrile with 0.1% formic acid as eluent A, and HPLC grade water with 0.1% formic acid as eluent B, at a flow rate of 1 mL/min. The elution gradient started with 2% eluent A, increasing to 40% in 10 min, and to 100% in the following 7 min. The % of eluent A was held constant at 100%

for the next 4 min before returning to the initial conditions and re-equilibrating the column. The total run time was 26 min.

The settings of the Turbo Ion Spray source operated in (+)ESI mode were: curtain gas 30 psi, nitrogen collision gas high, source temperature 700ºC, ion source gases GS1 and GS2 set at 62 V, and ion spray voltage of 5500 V. Full-scan analyses were performed in the mass range *m/z* 50-600. The declustering potential (DP) in the full scan experiments was 80 V, while DP and collision energy (CE) in the MS^2 and MS^3 experiments were optimized for each product and varied between 75-90 V and 20-40 eV, respectively. The injection volume was 20 µL. Samples were injected directly, without any pretreatment. In order to determine the degradation profiles of DOX, samples were diluted in ratio 1:20-1:10 with HPLC water, and analysed in multiple ion monitoring (MRM) mode, with transitions 271.2→182.1 (DP=40 V, CE=24 eV, cell exit potential (CXP)=8 V) and 271.2→167.1 (DP=40 V, CE=45 eV, CXP=7 V) as quantification and confirmation transitions, respectively.

Table S1 Proposed oxidation products of doxylamine (DOX): compound designation, molecular formula, calculated molecular weight (MW), retention time (t_R) and proposed structure.

Compound	Mol. formula	MW	t_R, min	Proposed structure
DOX	$C_{17}H_{22}N_2O$	270.17	8.5	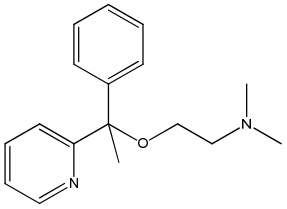
P105	$C_4H_{11}NO_2$	105.08	2.4	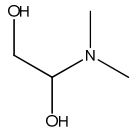
P89	$C_4H_{11}NO$	89.08	2.5	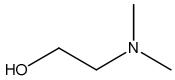
P131	$C_6H_{13}NO_2$	131.09	3.0	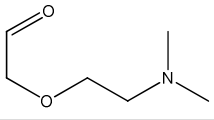
P135	$C_5H_{13}NO_3$	135.09	2.7, 3.2, 3.5, 4.0	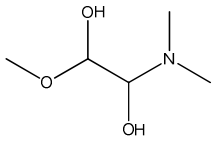
P95	C_5H_5NO	95.0	5.5	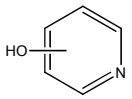
P169	$C_8H_{11}NO_3$	169.07	9.6, 10.5	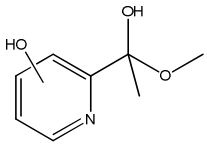
P155	$C_7H_9NO_3$	155.06	11.0	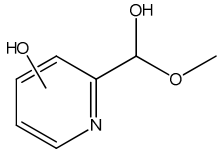
P181	$C_9H_{11}NO_3$	181.07	7.7, 8.5	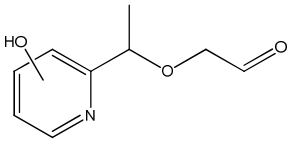

P199	$C_9H_{13}NO_4$	199.08	6.8	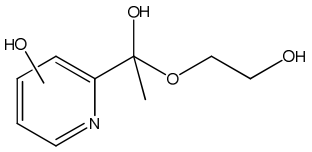
P197	$C_9H_{11}NO_4$	197.07	7.5	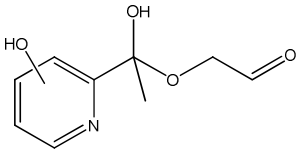
P286	$C_{17}H_{22}N_2O_2$	286.17	6.0, 6.1, 6.9	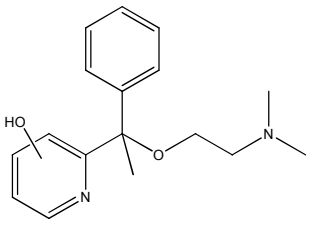
P209	$C_{12}H_{19}NO_2$	209.14	6.9, 7.2	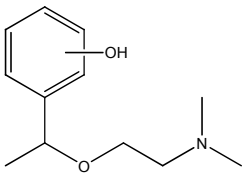
P235	$C_{14}H_{21}NO_2$	235.16	10.0	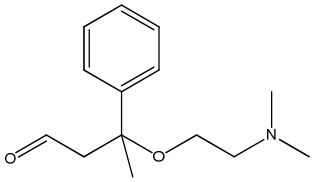
P237	$C_{13}H_{19}NO_3$	237.14	8.7	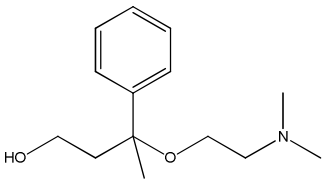
P275	$C_{16}H_{21}NO_3$	275.15	9.8	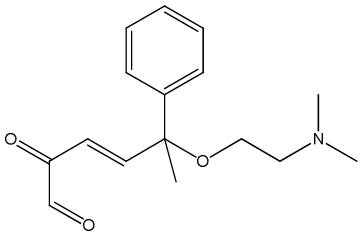
P293	$C_{16}H_{22}NO_4$	293.17	9.5	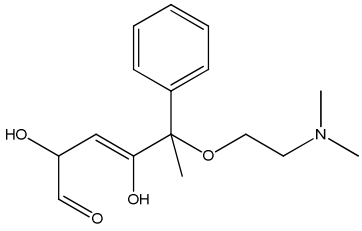

P291	$C_{16}H_{21}NO_4$	291.15	10.1	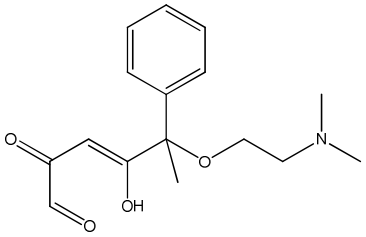
P327	$C_{16}H_{22}ClNO_4$	327.12	12.3	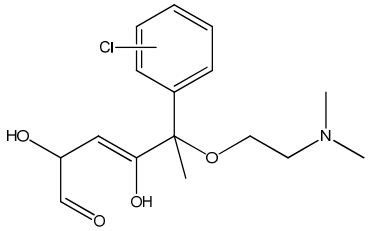
P325	$C_{16}H_{20}ClNO_4$	325.11	12.9, 13.0	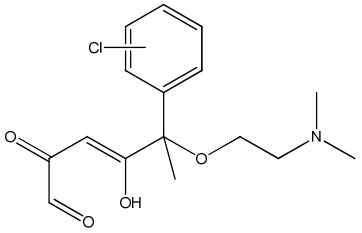
P304	$C_{17}H_{21}ClN_2O$	304.13	13.1, 13.5	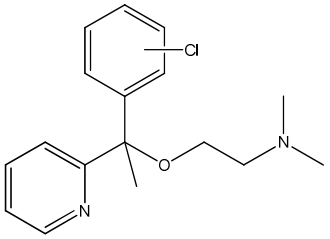
P303	$C_{14}H_{19}Cl_2NO_2$	303.08	13.1	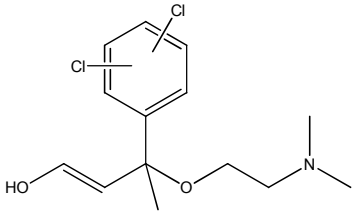

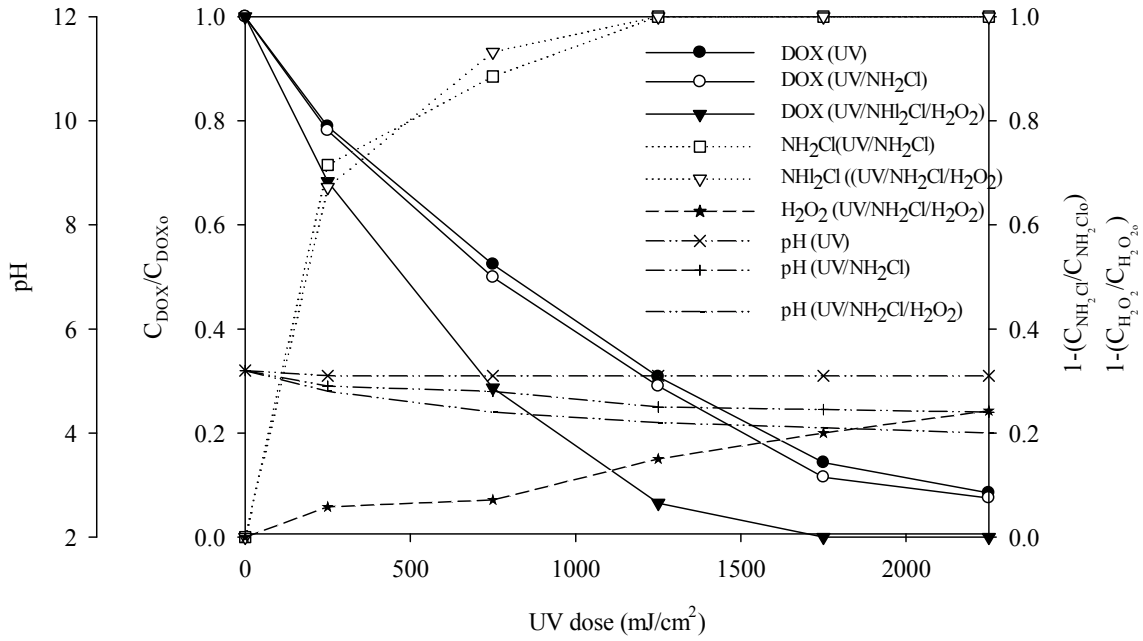

Figure S1. Relative concentration of doxylamine (DOX), NH_2Cl and H_2O_2 during UV, UV/NH_2Cl and UV/NH_2Cl/H_2O_2 treatment. $[NH_2Cl]_0$=20 mg/L, $[H_2O_2]_0$=50 mg/L, $[DOX]_0$=20 mg/L.

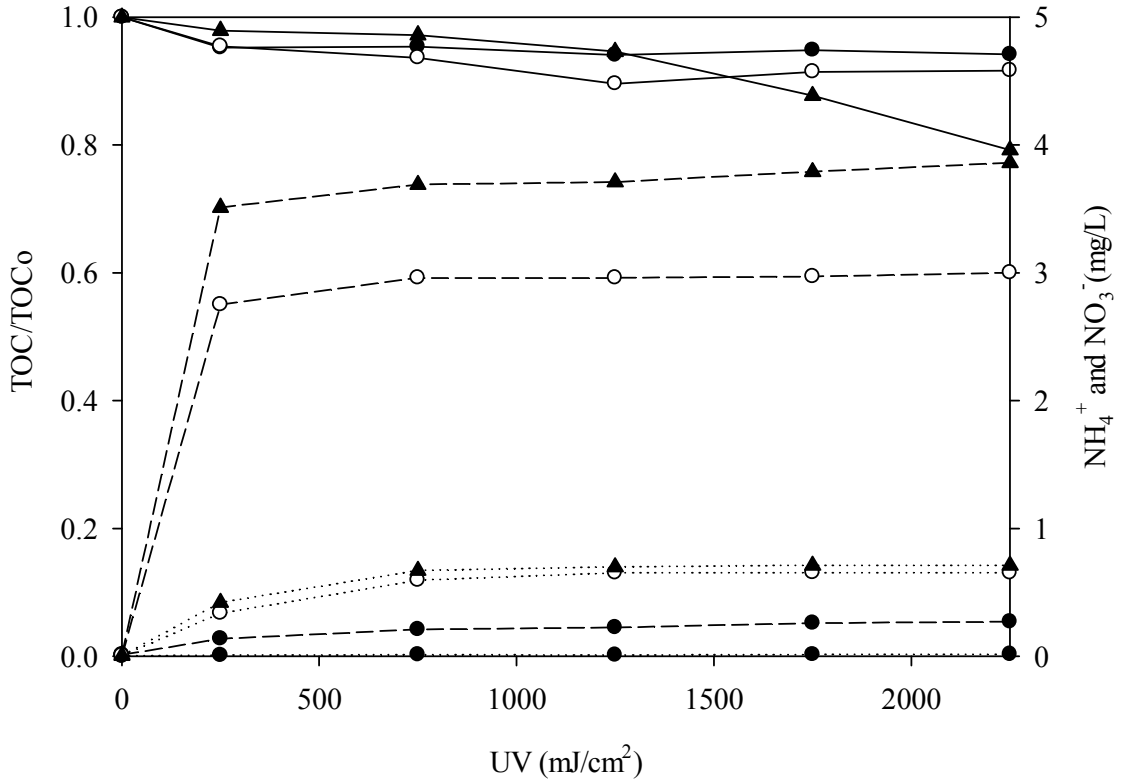

Figure S2 Relative concentration of TOC (solid), $N\text{-}NH_4^+$ (dashed) and $N\text{-}NO_3^-$ (dotted). (●) UV, (○) UV/NH_2Cl, and (▲) UV/NH_2Cl/H_2O_2.

Extracted ion chromatograms (XICs) of DOX and the identified oxidation products

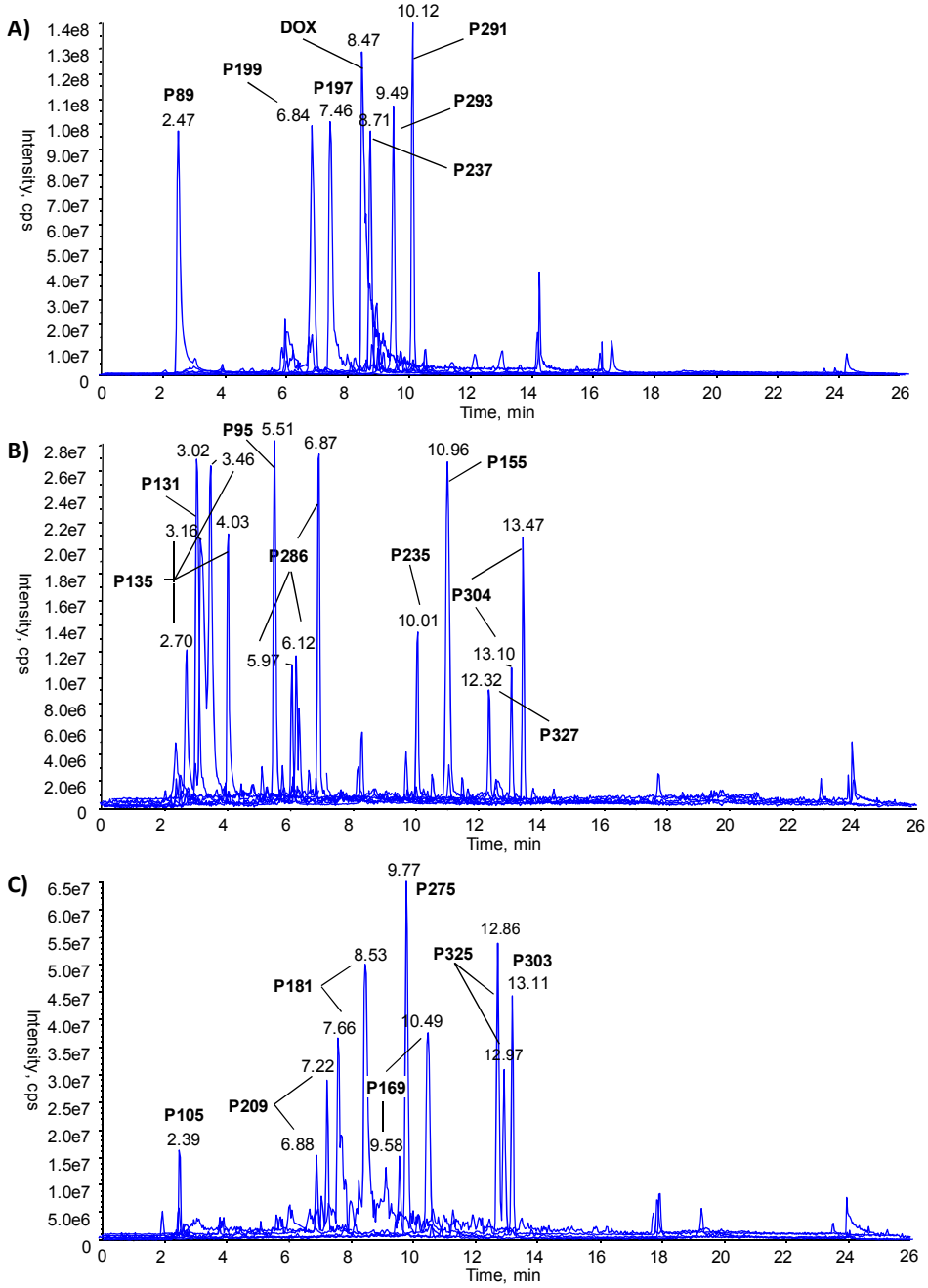

Figure S3 Extracted ion chromatograms (XICs) of DOX and its identified oxidation products, obtained by UFLC-(+)ESI-QqLIT-MS: **A)** DOX, P291, P293, P199 (sample UV, 25 min), P237 (UV, 35 min), P197, P89 (sample UV, 45 min), **B)** P286 (UV, 25 min), P95, P235, P155 (sample UV, 45 min), P327 (UV/NH_2Cl, 5 min), P304 (UV/NH_2Cl, 15 min), P131, P135 (UV/NH_2Cl/H2O2, 35 min), and **C)** P275, P181, P183 (UV, 25 min), P169, P209 (UV, 45 min), P303 (UV/NH_2Cl, 15 min), P105 (UV/NH_2Cl/H_2O_2, 35 min).

MS^2 and MS^3 spectra of DOX and the identified oxidation products

DOX

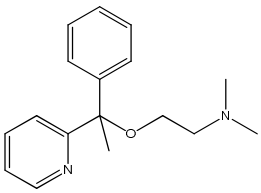

DOX eluted at t_R=8.5 min. The MS^2 spectrum of its molecular ion *m/z* 271 depicted in Figure S4 A showed a loss of 45 Da, i.e. the cleavage of the *N*,*N*-dimethylamino moiety (-$NH(CH_3)_2$), which yielded a fragment ion with *m/z* 226. Signals at *m/z* 72 and *m/z* 90 were derived from the ether bond scission and expulsion of *N*,*N*-dimethylethyleneamine and *N*,*N*-dimethylethanolamine ions, respectively, from the backbone of DOX. The high intensity fragment ion *m/z* 182 was isolated and further fragmented in an MS^3 experiment (Figure S4 B). Cleavage of the methyl group in *m/z* 182 gave rise to the radical base peak ion *m/z* 167. Another radical fragment ion *m/z* 140 was generated by a further expulsion of HCN from *m/z* 167, which is typical for mass spectra of pyridine moieties [4]. The spectra obtained for DOX are in accordance with the previously reported results of thermospray/tandem mass spectrometry analyses of DOX [5].

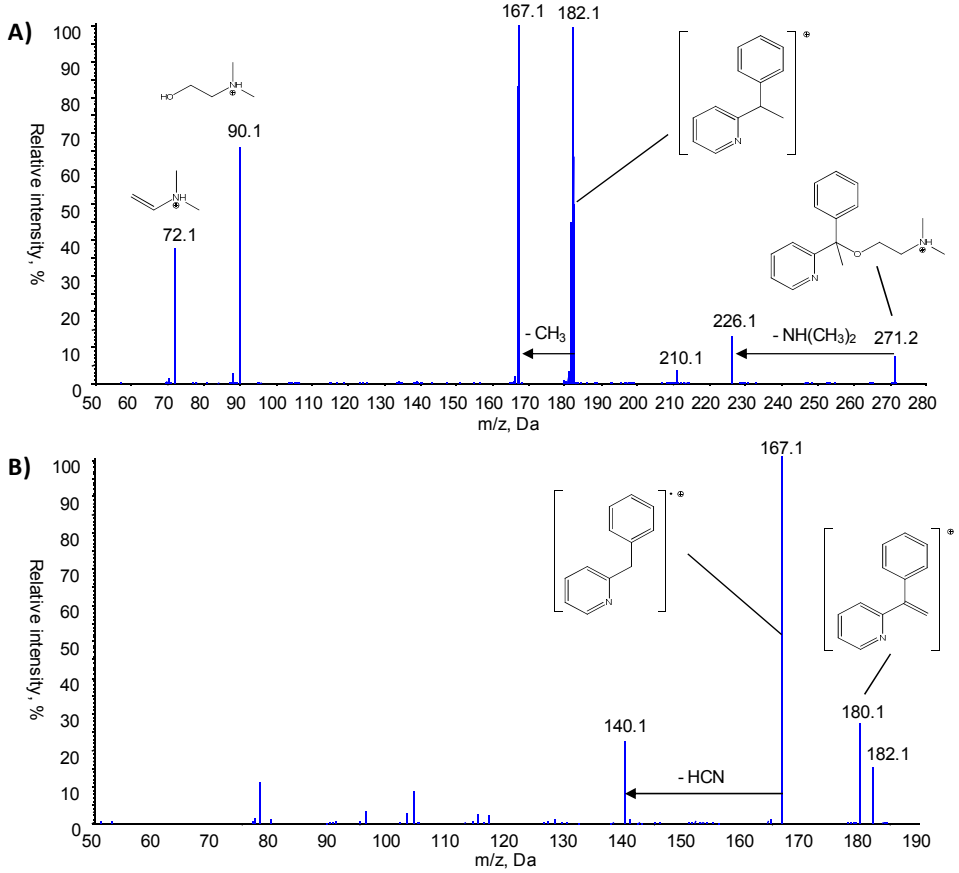

Figure S4 A) (+)ESI-QqLIT-MS^2 spectrum of DOX, *m/z* 271.2, **B)** (+)ESI-QqLIT-MS^3 spectrum: *m/z* 271.2→*m/z* 182.1.

P95

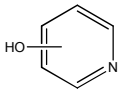

Product P95 (molecular ion *m/z* 96) at t_R=5.5 min exhibited the MS^2 spectrum of a hydroxylated pyridine ring (Figure S5 A). The MS^3 spectrum *m/z* 96→*m/z* 78 (Figure S5 B) contained a signal at *m/z* 51, corresponding to the loss of HCN typical of pyridine moieties [6].

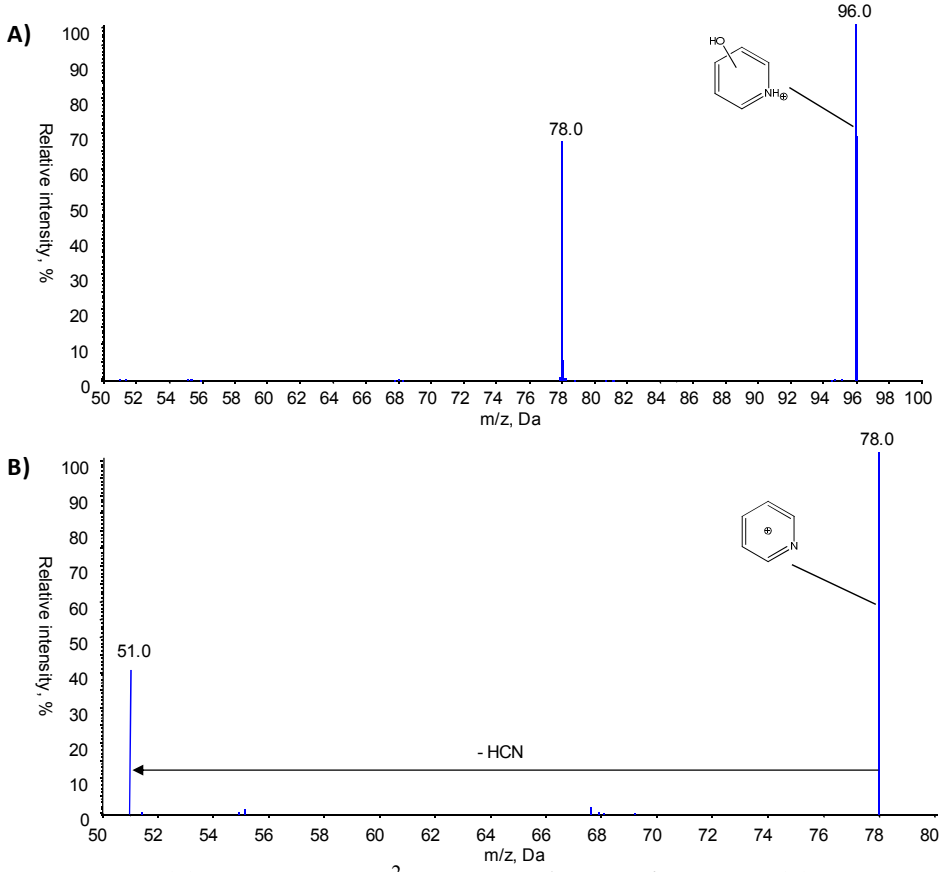

Figure S5 A) (+)ESI-QqLIT-MS^2 spectrum of P95, *m/z* 96.0, **B)** (+)ESI-QqLIT-MS^3 spectrum: *m/z* 96.0→*m/z* 78.0.

P169

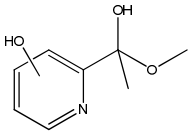

Figure S5 depicts the MS^2 and MS^3 spectra of product P169 (t_R=9.6 and 10.5 min), with a molecular ion *m/z* 170. The formation of fragment ions *m/z* 155 and *m/z* 154 could be rationalized by cleavage of $–CH_3$ group, typical of methyl ethers [6], and elimination of oxygen from the quaternary C atom of the molecular ion *m/z* 170, respectively (Figure S6 A). Similar to the spectra of DOX and P95, expulsion of HCN from the pyridine moiety resulted in the signal at *m/z* 143. Furthermore, in the MS^2 spectrum of *m/z* 170, fragment ions *m/z* 78 (pyridine ion) and *m/z* 96 (hydroxylated pyridine ion) could be discerned. Product ion *m/z* 110 was identified as a hydroxylated methyl pyridine (picoline) ion $C_6H_8NO^+$, as confirmed by the MS^3 spectrum *m/z* 170→*m/z* 154 (Figure S6 B). Furthermore, the proposed structure

of fragment ion *m/z* 143 was corroborated by the MS^3 spectrum *m/z* 170→*m/z* 143 (Figure S6 C) with the base peak ion *m/z* 128 derived from the scission of the -CH_3 from the methoxy group, and fragment ions *m/z* 127 and *m/z* 117 obtained by the loss of oxygen from the quaternary C atom, and likely a –C_2H_2 group in *m/z* 143.

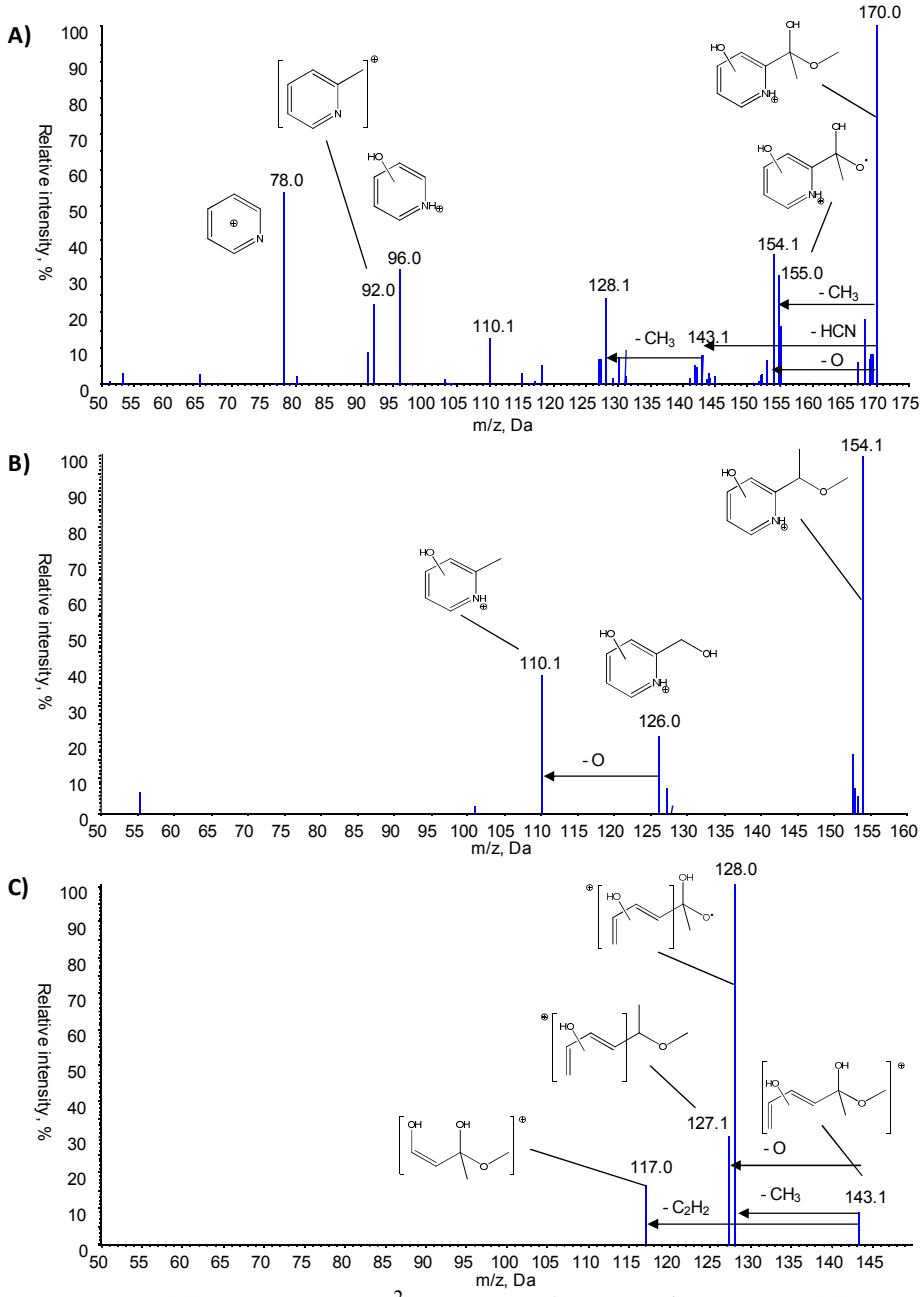

Figure S6 A) (+)ESI-QqLIT-MS^2 spectrum of P169, *m/z* 170.0, **B)** (+)ESI-QqLIT-MS^3 spectrum: *m/z* 170.0→*m/z* 154.1, and **C)** (+)ESI-QqLIT-MS^3 spectrum: *m/z* 170.0→*m/z* 143.1.

Considering the low MW of P169 and the presence of two –OH groups, a lower t_R could be expected for P169. However, the 3D-structure of proposed P169 obtained in a ChemBio 3D Ultra 12.0 suite [7] indicated a high geometrical probability for an intra-molecular hydrogen bond between the aliphatic –OH and the ether group, which is possibly the reason for its late appearance in the chromatogram. Influence of intra-molecular hydrogen bonds on the order

of LC elution of hydroxylated derivatives was previously observed in [8, 9]. Additionally, the attachment of –OH in the α-position of the side chain could have contributed to the decreased polarity of P169 by an additional intra-molecular hydrogen bonding with the ether group. However, the exact position of the –OH substituent of the pyridine moiety could not be determined.

P155

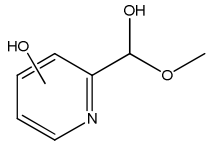

Product P155 (molecular ion *m/z* 156) eluted at t_R=11.0 min. As in the case of P169, the MS^2 spectrum of *m/z* 156 contained signals at *m/z* 78 and *m/z* 96, diagnostic of the hydroxylated pyridine ring (Figure S7 A). Neutral loss of HCN (27 Da) and CO (28 Da) yielded the fragment ions *m/z* 129 and *m/z* 128, respectively. Product ion *m/z* 129 was further collisioned in the MS^3 experiments (Figure S7 B) giving rise to a signal at *m/z* 114, formed by the loss of a methyl radical, which is characteristic for methoxy groups. While elimination of HCN is characteristic for the mass spectra of pyridines [10], loss of CO is characteristic for both, phenol moieties [6] and some hydroxypyridines [10]. Namely, mass spectral pattern of hydroxypyridines may involve the expulsion of HCN, CO upon the tautomerisation in the ion source, or in some cases both molecules [10], depending on the position of the –OH group and other substituents.

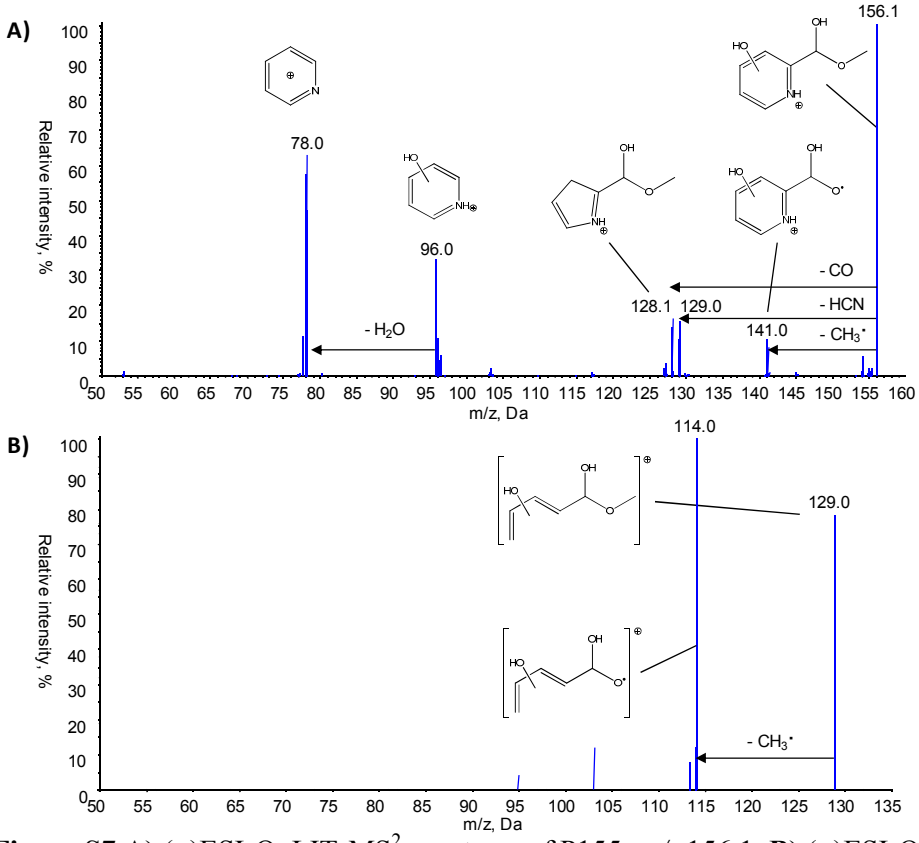

Figure S7 A) (+)ESI-QqLIT-MS^2 spectrum of P155, *m/z* 156.1, **B)** (+)ESI-QqLIT-MS^3 spectrum: *m/z* 156.1→*m/z* 129.0.

P181

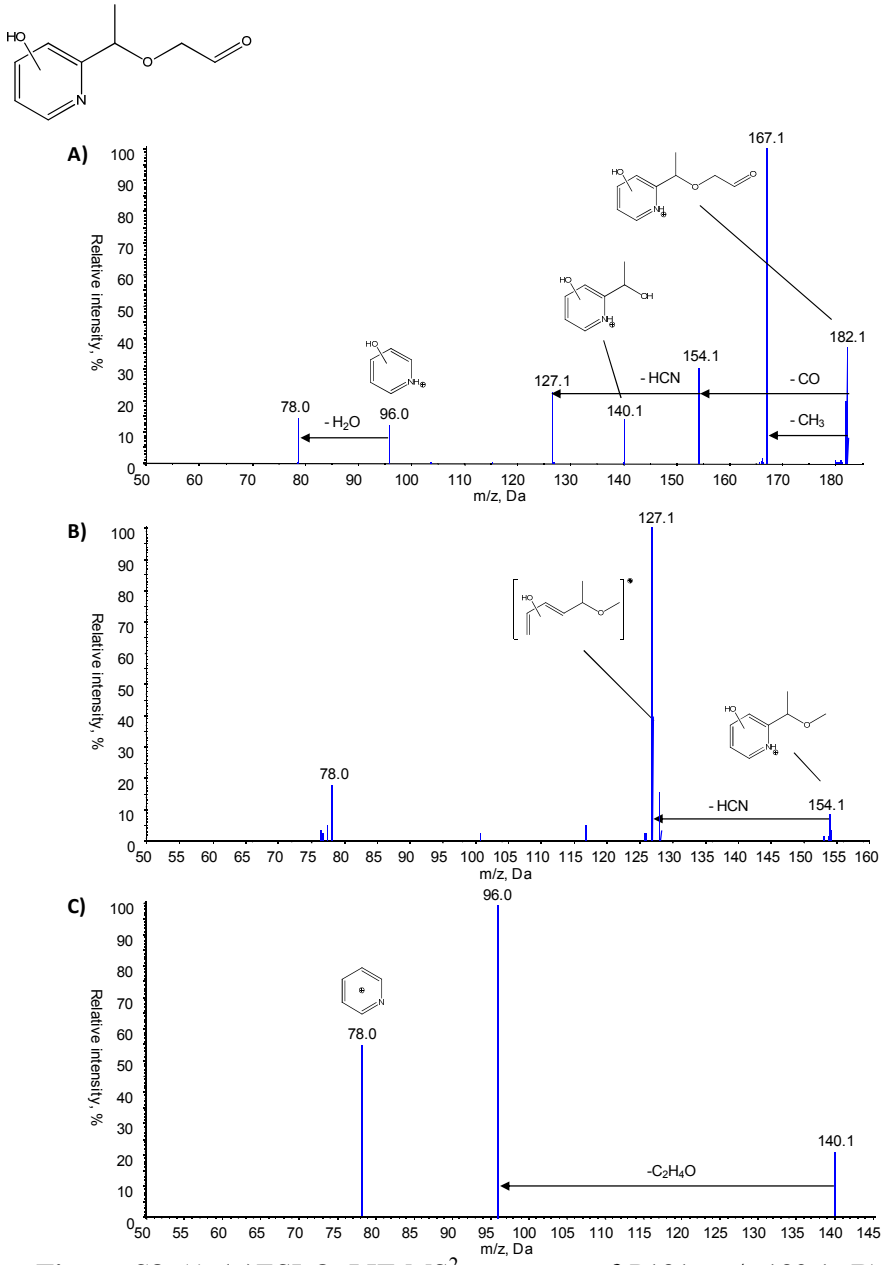

Figure S8 A) (+)ESI-QqLIT-MS^2 spectrum of P181, *m/z* 182.1, **B)** (+)ESI-QqLIT-MS^3 spectrum: *m/z* 182.1→*m/z* 154.1, and **C)** (+)ESI-QqLIT-MS^3 spectrum: *m/z* 182.1→*m/z* 140.1.

Two peaks with t_R=7.7 and 8.5 min with identical mass spectra (Figure S8) were found for product P181, with a molecular ion *m/z* 182. Fragmentation of *m/z* 182 displayed diagnostic ion *m/z* 96, implying the hydroxylation of the pyridine ring (Figure S8 A). On the other hand, initial neutral losses of 28 Da and 15 Da were assigned to the elimination of CO and homolytic scission of a methyl group in *m/z* 182. Further loss of HCN (27 Da) from the pyridine ring of *m/z* 154 was highly favoured in the MS^3 spectrum *m/z* 182→*m/z* 154 (Figure S8 B), resulting in a base peak ion *m/z* 127. The presence of pyridine ion at *m/z* 78 in this spectrum indicated that the fragmentation *m/z* 182→*m/z* 154 had occurred by the scission of a

terminal carbonyl group, and not as expulsion of CO form the hydroxylated pyridine ring. Furthermore, product ion *m/z* 140 was likely formed by the scission of the ether bond, which was corroborated by the MS^3 fragmentation *m/z* 182→*m/z* 140 (Figure S8 C). Therefore, P181 was determined to be formed by the hydroxylation of pyridine ring in DOX and oxidative cleavages of benzene and *N,N*-dimethylamino group.

P199

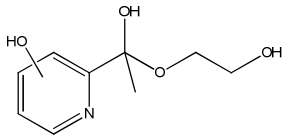

Product P199, with a molecular ion *m/z* 200, emerged at t_R=6.8 min. The initial losses of 15 Da (*m/z* 185) and 18 Da (*m/z* 182) in the MS^2 fragmentation of *m/z* 200 (Figure S9 A) were attributed to the scission of $–CH_3$ group and expulsion of H_2O, respectively. Additionally, neutral loss of 30 Da was noted, which gave rise to fragment ion *m/z* 170. Isolation and further fragmentation of *m/z* 170 (Figure S9 B) yielded a base peak ion *m/z* 156 and fragment ion *m/z* 143, hypothesized to be formed by a cleavage of $–CH_2$ group and elimination of HCN, respectively. Also, diagnostic signals at *m/z* 78 and *m/z* 96 were recorded. Based on the spectrum in Figure S8 B, a plausible structure of product ion *m/z* 170 was traced back to the scission of –CHOH from the primary alcohol in *m/z* 200. Product ion *m/z* 154 appearing in the MS^3 spectrum of *m/z* 200→*m/z* 182 (Figure S9 C) was presumably generated by the cleavage of ether bond and expulsion ethylene. Finally, expulsion of HCN from the pyridine ring in *m/z* 154 gave rise to the base peak ion *m/z* 127.

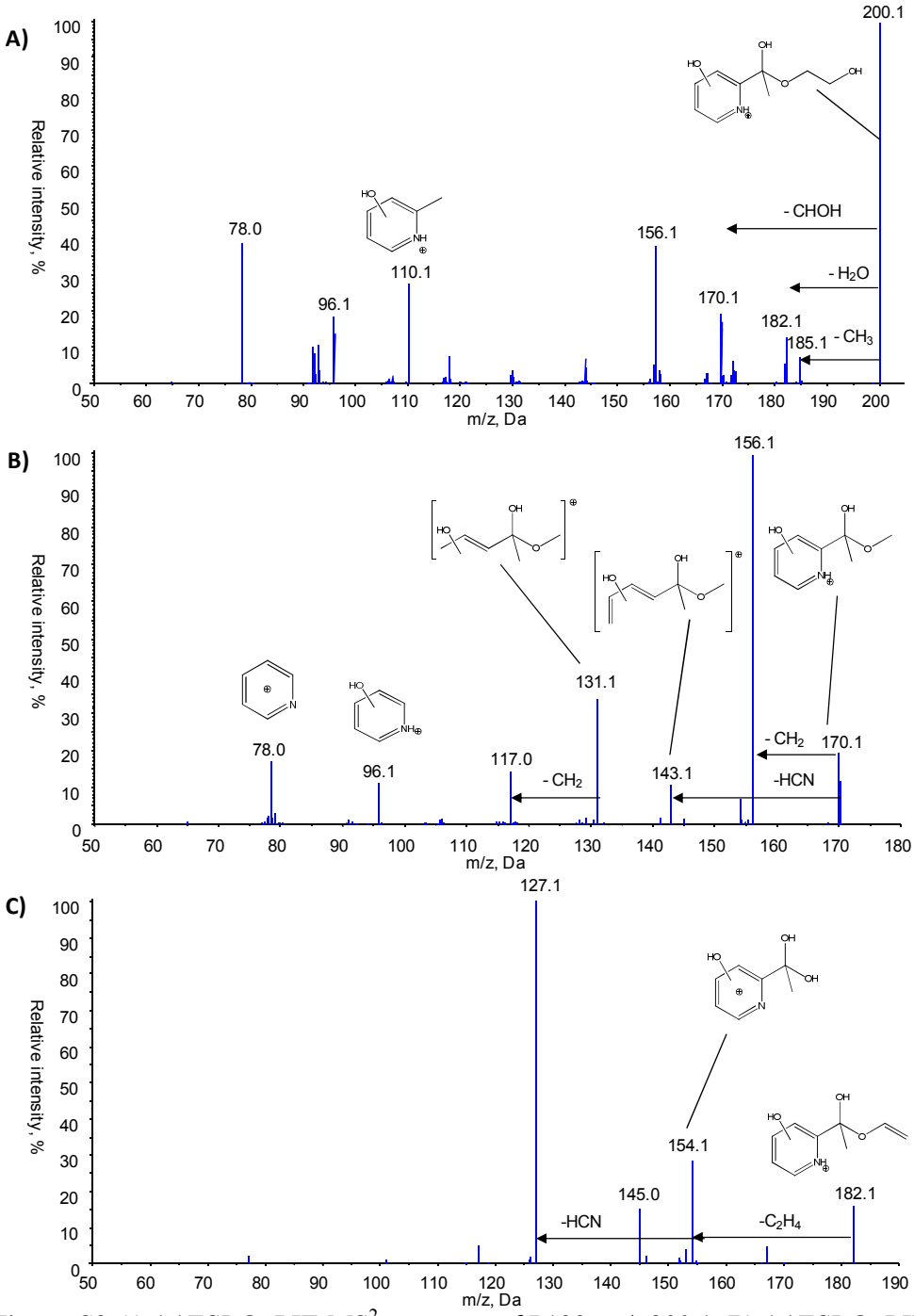

Figure S9 A) (+)ESI-QqLIT-MS^2 spectrum of P199, *m/z* 200.1, **B)** (+)ESI-QqLIT-MS^3 spectrum: *m/z* 200.1→*m/z* 182.1, and **C)** (+)ESI-QqLIT-MS^3 spectrum: *m/z* 200.1→*m/z* 170.1.

P197

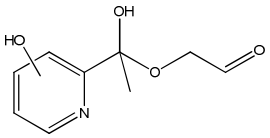

Concomitantly with P199 appeared its carbonyl-form, product P197, at t_R=7.5 min and exhibited the MS^2 spectrum shown in Figure S10 A. The molecular ion *m/z* 198 underwent three characteristic losses of 15 Da (*m/z* 183), 18 Da (*m/z* 180) and 28 Da (*m/z* 170) assigned to elimination of $–CH_3$, H_2O and CO, respectively. The presumed structure of P197 was corroborated by the isolation and further fragmentation of product ion *m/z* 180 (Figure S10 B) and *m/z* 170 (Figure S10 C). Fragment ions *m/z* 180 was determined to be the precursor for ion *m/z* 152, obtained by the cleavage of the terminal CO group. On the other hand, MS^3 spectrum *m/z* 198→*m/z* 170 contained a base peak ion *m/z* 156 ($-CH_2$), hydroxylated picoline ion *m/z* 110 and ion *m/z* 96.

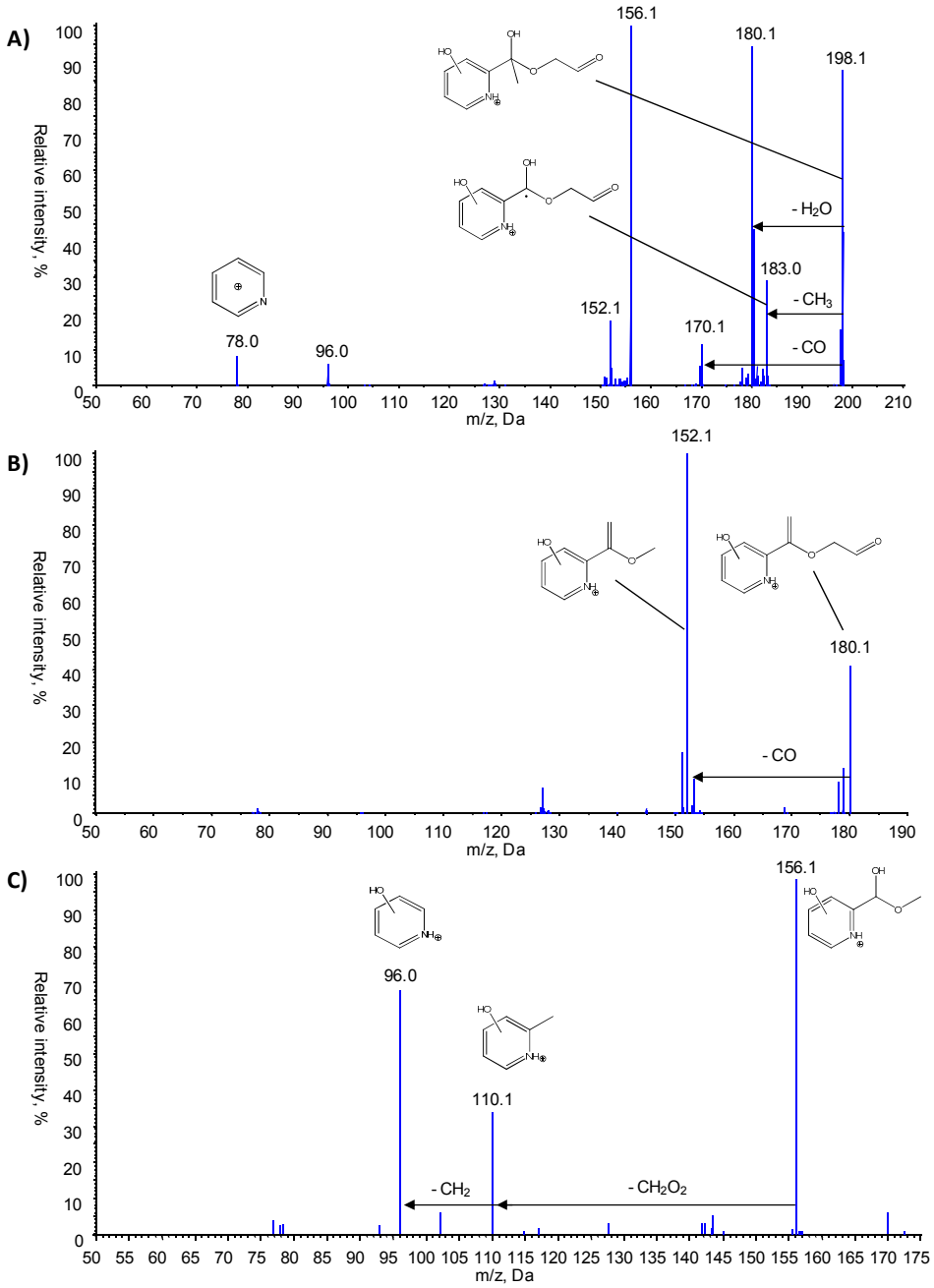

Figure S10 A) (+)ESI-QqLIT-MS^2 spectrum of P197, *m/z* 198.1, **B)** (+)ESI-QqLIT-MS^3 spectrum: *m/z* 198.1→*m/z* 180.1, and **C)** (+)ESI-QqLIT-MS^3 spectrum: *m/z* 198.1→*m/z* 170.1.

P286

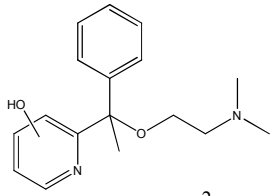

Based on its MS^2 and MS^3 spectra presented in Figure S11 A and B, product P286 with a molecular ion *m/z* 287 was identified as a hydroxylated derivative of DOX. Absence of a

neutral loss of water (18 Da), typical of aliphatic –OH substituents, and recording of fragment ions *m/z* 90 and *m/z* 72 in the MS^2 spectrum of *m/z* 287 (Figure S11 A) indicated that the –OH group was located at the phenyl or pyridine ring. In accordance with this assumption, the base peak ion *m/z* 198 and product ion *m/z* 183 were shifted for +16 Da relative to the ions *m/z* 182 and *m/z* 167 in the spectra of DOX, respectively. Nevertheless, the signal detected at *m/z* 110 indicated hydroxylation of the pyridine ring. It is known that although pyridines are less reactive than benzenes in electrophilic substitution, they are more reactive in the reactions of free-radical substitution. Therefore, P286 was hypothesized to correspond to a pyridine-hydroxylated derivative of DOX. In the MS^3 spectrum *m/z* 287→*m/z* 198 (Figure S11 B), fragment ion *m/z* 183 underwent further losses of 27 (HCN) and 28 Da (CO) that yielded product ions *m/z* 156 and *m/z* 155, respectively.

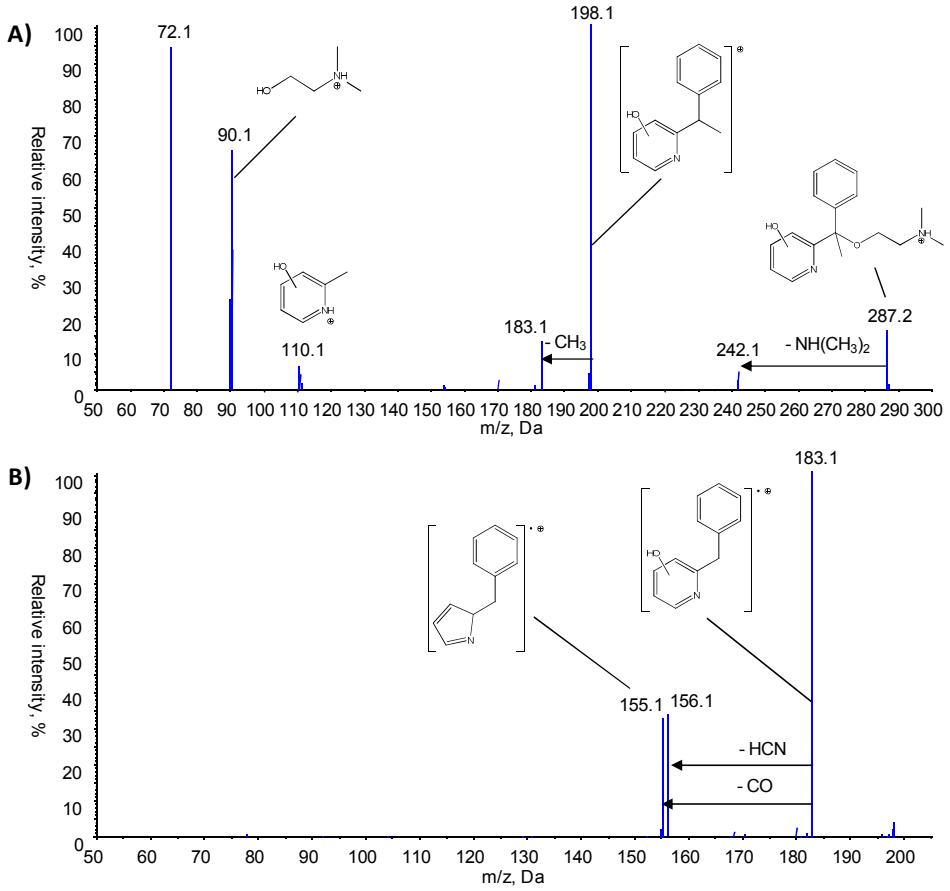

Figure S11 A) (+)ESI-QqLIT-MS^2 spectrum of P286, *m/z* 287.2, **B)** (+)ESI-QqLIT-MS^3 spectrum: *m/z* 287.2→*m/z* 198.1.

P209

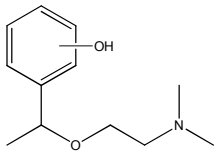

Peaks eluting at t_R=6.9 and 7.2 min displayed a molecular ion *m/z* 210 and the fragmentation pattern presented in Figures S12 A and B. Neutral loss of 45 Da (i.e. fragment ion *m/z* 165) and signals at *m/z* 90 and *m/z* 72 indicated that the side chain of DOX remained unchanged.

On the other hand, low intensity fragment ion *m/z* 182 was generated by a loss of 28 Da assigned to an expulsion of CO, typical in the mass spectra of phenol moieties [6]. Cleavage of the ether bond in sequential fragmentation of *m/z* 210→*m/z* 165 (Figure S12 B) resulted in a loss of vinyl alcohol group (-CH_2CHOH) and formation of *m/z* 121. Additionally, benzene, toluene and phenol ion were recorded at *m/z* 77, *m/z* 91 and *m/z* 93, respectively.

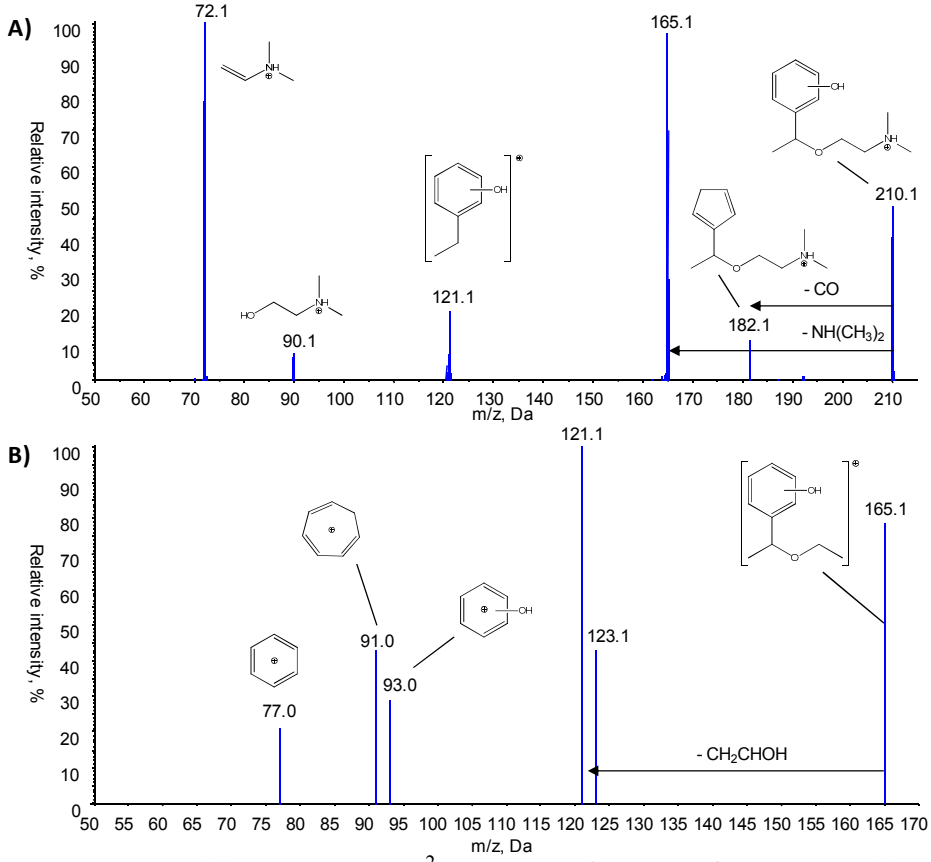

Figure S12 A) (+)ESI-QqLIT-MS^2 spectrum of P209, *m/z* 210.1, **B)** (+)ESI-QqLIT-MS^3 spectrum: *m/z* 210.1→*m/z* 165.1.

P235

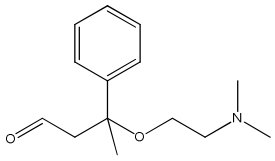

Product P235 eluted at t_R=10.0 min characterized by the fragmentation pattern in Figure S12. The product ion profile of the molecular ion *m/z* 236 (Figure S13 A) contained fragment ions *m/z* 90 and *m/z* 72, and showed a loss of 45 Da (fragment ion *m/z* 191), characteristic of the *N*,*N*-dimethylethyleneamine side chain. The base peak ion at *m/z* 147 was hypothesized to originate from the cleavage of the ether bond and expulsion of the vinyl alcohol moiety (-CH_2CHOH) from the side chain of ion *m/z* 191, similar to the spectra of P209 in Figure S12 B. Further loss of 28 Da (product ion *m/z* 119) was assigned to an expulsion of a terminal CO group. This hypothesis was additionally confirmed by detecting the hydroxylated form of P235, product P237, explained further in the text. A plausible structure of the base peak ion *m/z* 135 in the MS^3 spectrum *m/z* 236→*m/z* 191 (Figure S13 B) was derived from the scission of side chain and methyl group in the molecular ion *m/z* 236. This was corroborated by the

MS^3 of *m/z* 135 (Figure S12 C), which gave rise to the aromatic product ion *m/z* 105 and the benzene ion *m/z* 77.

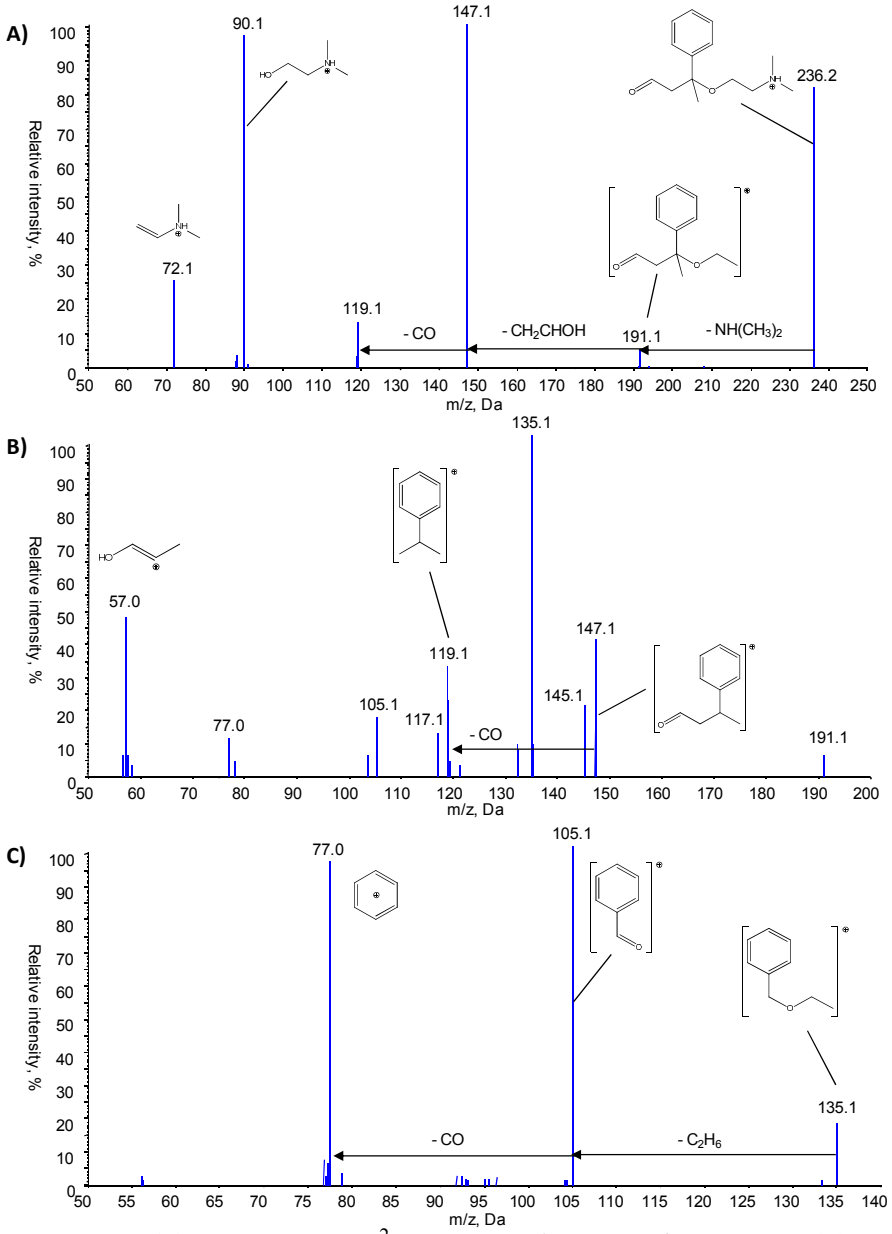

Figure S13 A) (+)ESI-QqLIT-MS^2 spectrum of P235, *m/z* 236.2, **B)** (+)ESI-QqLIT-MS^3 spectrum: *m/z* 236.2→*m/z* 191.1, and **C)** (+)ESI-QqLIT-MS^3 spectrum: *m/z* 236.2→*m/z* 135.1.

P237

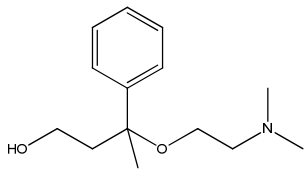

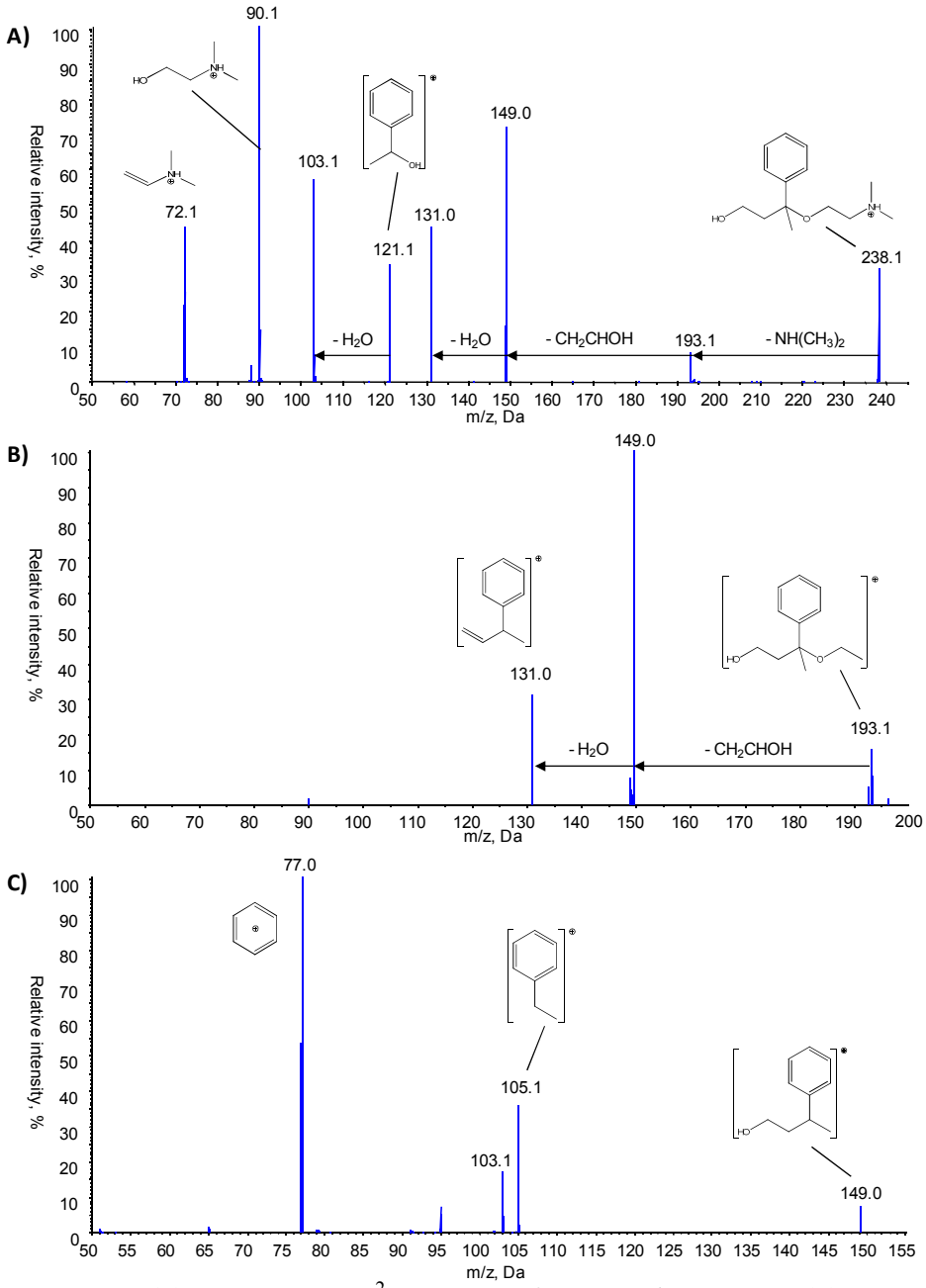

Figure S14 A) (+)ESI-QqLIT-MS^2 spectrum of P237, *m/z* 238.1, **B)** (+)ESI-QqLIT-MS^3 spectrum: *m/z* 238.1→*m/z* 149.0, and **C)** (+)ESI-QqLIT-MS^3 spectrum: *m/z* 238.1→*m/z* 193.1.

Collision induced dissociation (CID) fragmentation of the molecular ion *m/z* 238 (t_R=8.7 min) gave rise to a mass spectrum in Figure S14 A. The base peak ion in the MS^2 spectrum of P237 was aliphatic *N,N*-dimethylethanolamine ion *m/z* 90. Consecutive neutral losses of 45 Da (*m/z* 193) and 44 Da (*m/z* 149) were observed, postulated to represent the cleavages of–$NH(CH_3)_2$ and -CH_2CHOH groups, respectively, from the side chain of P237. This was confirmed by selecting the product ion *m/z* 193 in the MS^3 fragmentation (Figure S14 B). This fragmentation also yielded a signal at *m/z* 131 obtained by a further elimination of water from *m/z* 149, which is characteristic of primary alcohols [6]. In the MS^3 spectrum *m/z*

238→*m/z* 149 (Figure S14 C) the benzene ion *m/z* 77 as the base peak ion and two aromatic fragment ions *m/z* 105 and *m/z* 103 were noted.

P275

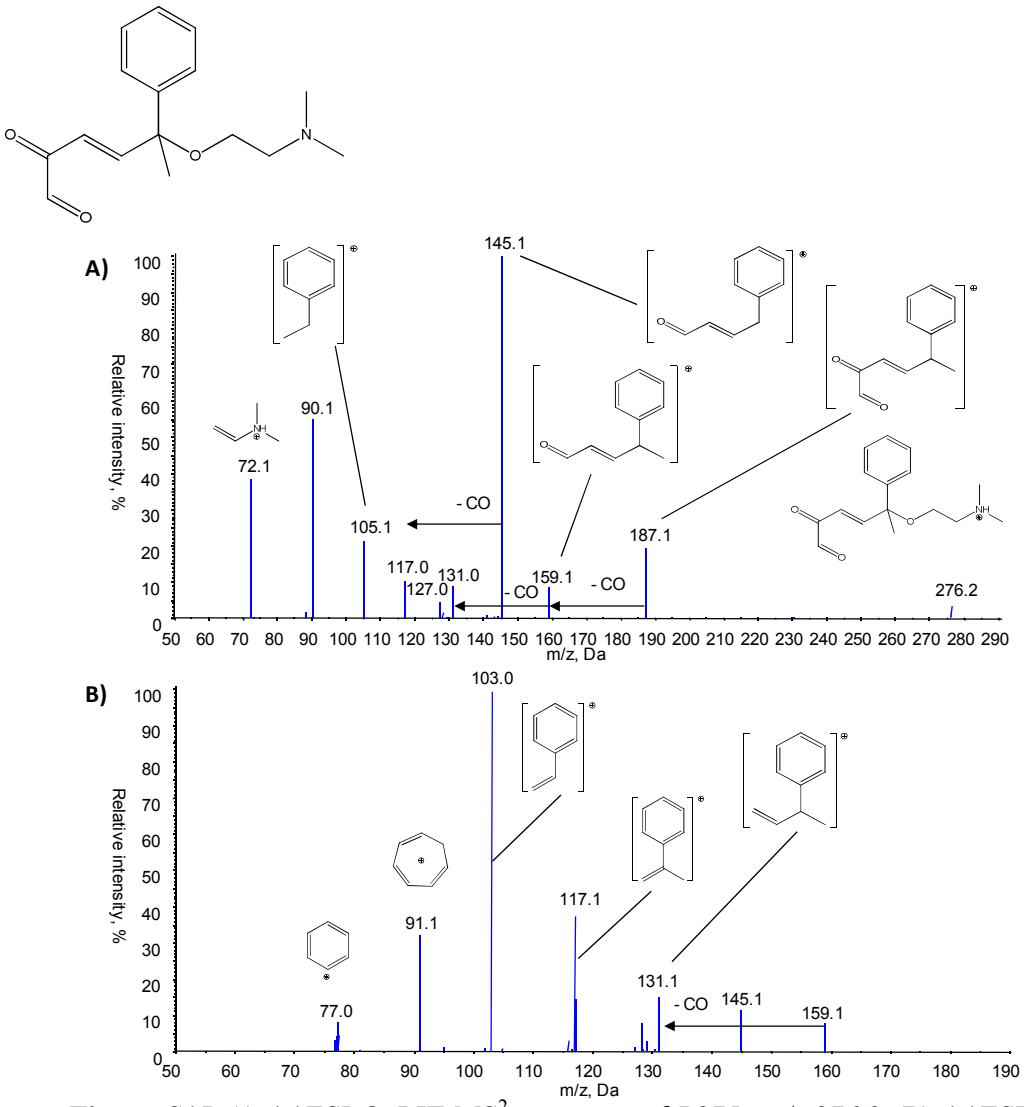

Figure S15 A) (+)ESI-QqLIT-MS^2 spectrum of P275, *m/z* 276.2, **B)** (+)ESI-QqLIT-MS^3 spectrum: *m/z* 276.2→*m/z* 187.1.

Product P275 (molecular ion *m/z* 276) eluted at t_R=9.8 min. The MS^2 fragmentation pattern of *m/z* 276 (Figure S15 A) contained fragment ions *m/z* 72 and *m/z* 90, as well as loss of 89 Da (fragment ion *m/z* 187), characteristic of the *N,N*-dimethylethyl amine backbone. Formation of ions *m/z* 159 and *m/z* 131 was interpreted as two subsequent eliminations of CO molecules from *m/z* 187, as confirmed by the MS^3 experiments of *m/z* 276→*m/z* 187 (Figure S15 B). This fragmentation also yielded the aromatic ions *m/z* 117, *m/z* 113, *m/z* 91 (toluene) and *m/z* 77 (benzene ion).

P293

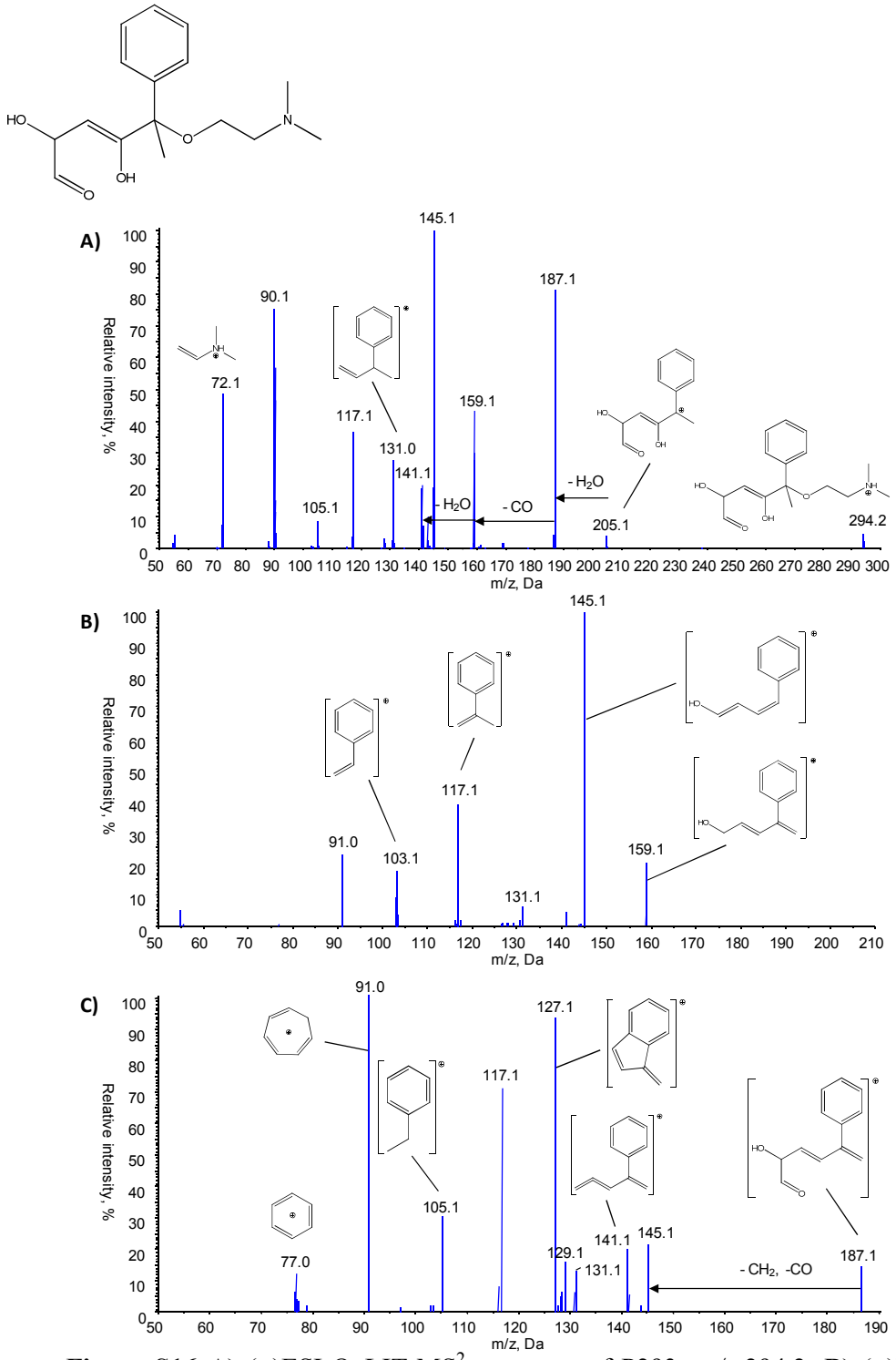

Figure S16 A) (+)ESI-QqLIT-MS^2 spectrum of P293, *m/z* 294.2, **B)** (+)ESI-QqLIT-MS^3 spectrum: *m/z* 294.2→*m/z* 205.1, and **C)** (+)ESI-QqLIT-MS^3 spectrum: *m/z* 294.2→*m/z* 187.1.

A peak with the molecular ion *m/z* 294 was noted at t_R=9.5 min (P293). Similar to the spectrum of P275 (Figure S15 A), *m/z* 294 underwent a loss of 89 Da through the cleavage of

the ether bond (Figure S16 A). Additionally, mass traces at *m/z* 90 and *m/z* 72 suggested an intact side chain in P293. In accordance with the nitrogen rule of mass spectrometry [6], P293 contained only the nitrogen atom in $–NH(CH_3)_2$ moiety, implying that the generation of P293 involved oxidative cleavages of pyridine ring. Subsequent expulsion of H_2O from product ion *m/z* 205 gave rise to a signal at *m/z* 187. The MS^3 spectrum *m/z* 294→*m/z* 205 (Figure S16 B) contained a signal at *m/z* 159, exhibiting a loss of 28 D that was assigned to a terminal CO group. The base peak ion *m/z* 145 was likely obtained by a loss of water from *m/z* 159. On the other hand, selection and further activation of product ion *m/z* 187 resulted in the fragmentation pattern in Figure S15 C. The plausible structure of the ion *m/z* 127 was traced back to the elimination of $-CH_2$ group in *m/z* 141 and intra-molecular cyclization. The signal at *m/z* 131 could be explained by the keto-enol tautomerism of *m/z* 159 in the source and expulsion of a terminal CO group. Keto-enol tautomerism in the ion source of electrospray (ESI) interfaces was previously observed in [11, 12].

P291

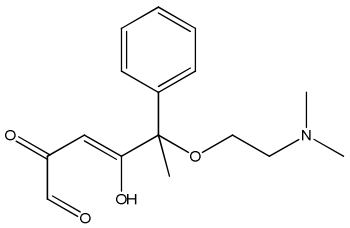

In parallel with the appearance of P293, another product with a molecular ion *m/z* 292 eluted at t_R=10.1 min The scrutiny of the MS^2 fragmentation pattern of P291 (Figure S17 A) revealed a shift in mass traces of -2 Da relative to the one observed for P293. Therefore, P291 was identified as a keto-form of P293. Specific pattern with shifts of 28 Da between high intensity signals *m/z* 185→*m/z* 157→*m/z* 129 suggested that the keto-group may be located at the cleaved pyridine ring. Furthermore, loss of 16 Da in the MS^3 spectrum *m/z* 292→*m/z* 185 (Figure S17 B) and formation of product ion *m/z* 169 was hypothesized to correspond to a loss of oxygen, possibly through keto-enol tautomerisation of *m/z* 169 and expulsion of –O from the –OH tautomer. The base peak ion *m/z* 107 in the spectrum in Figure S17 B was likely formed by a neutral loss of benzene (78 Da, C_6H_6) from *m/z* 185. Generation of the product ion *m/z* 79 could be explained either by the loss of the terminal CO from *m/z* 107, or the expulsion of water from the fragment ion *m/z* 97. Isolation of *m/z* 203 as a precursor ion in the MS^3 experiments (Figure S17 C) gave rise to ions *m/z* 157, *m/z* 131, and *m/z* 129 (further loss of CO from *m/z* 157), but also other aromatic ions such as *m/z* 143, *m/z* 115, and toluene ion. Scission of terminal $–CH_2$ group and CO in ion *m/z* 185 likely yielded the signal at *m/z* 143, and upon further loss of CO product ion *m/z* 115. Additionally, the toluene ion at *m/z* 91 and the ethylbenzene ion *m/z* 105 were also recorded.

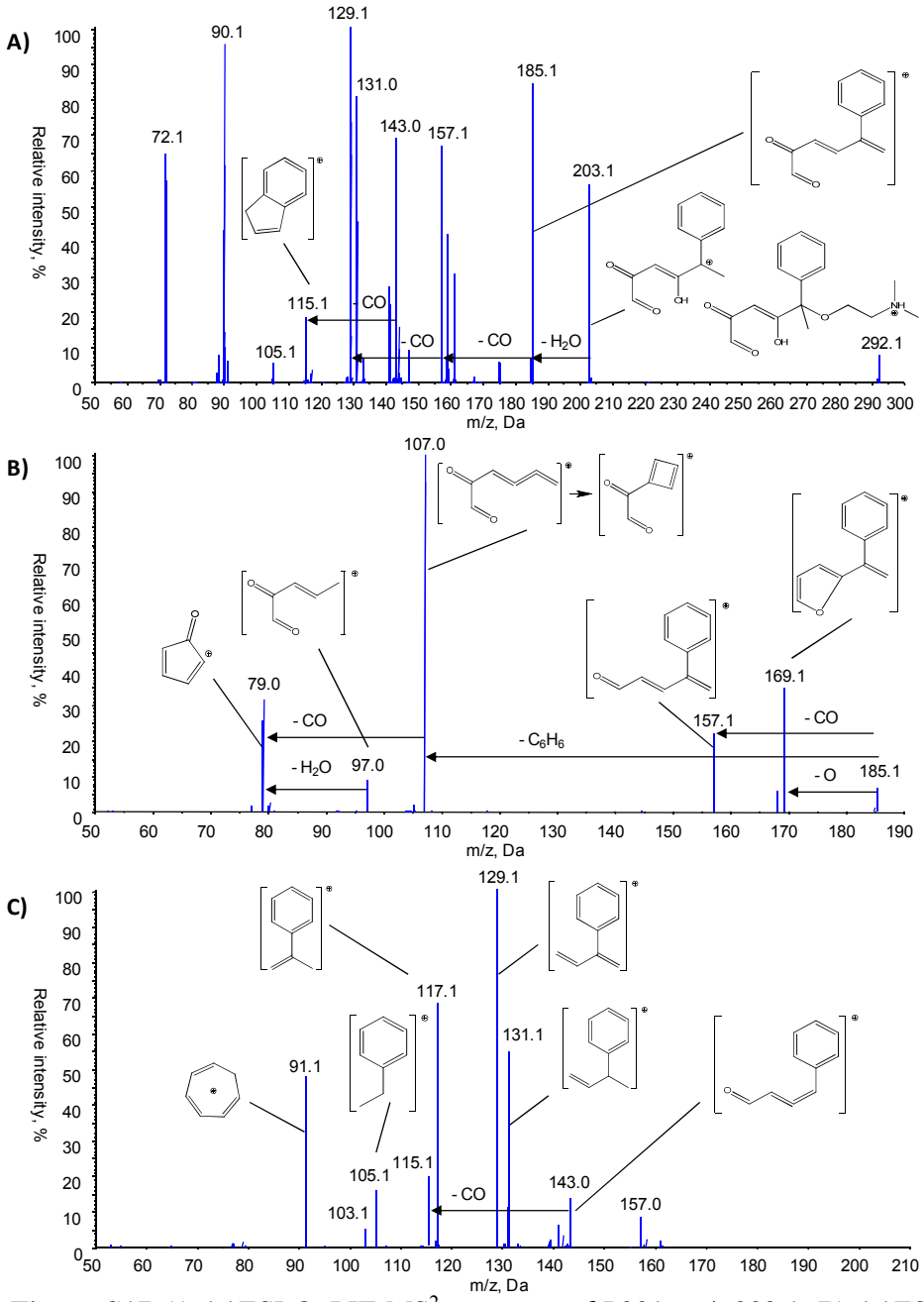

Figure S17 A) (+)ESI-QqLIT-MS^2 spectrum of P291, *m/z* 292.1, **B)** (+)ESI-QqLIT-MS^3 spectrum: *m/z* 292.1→*m/z* 185.1, and **C)** (+)ESI-QqLIT-MS^3 spectrum: *m/z* 292.1→*m/z* 203.1.

P327

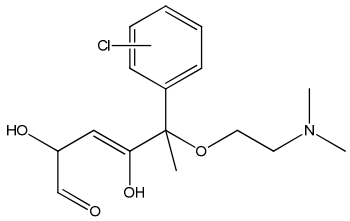

In the full-scan analyses of samples from the UV/NH_2Cl oxidation experiments, another peak emerged at t_R=12.3 min, determined to be a monochlorinated derivative of P293, product P327. Fragment ions *m/z* 239, *m/z* 221, *m/z* 193, and *m/z* 163 in the MS^2 spectrum of P327 (Figure S18 A) were equivalent to ions *m/z* 205, *m/z* 187, *m/z* 159 and *m/z* 129, respectively, observed for P293. Fragment ion *m/z* 203 was formed by the expulsion of HCl from the chlorinated benzene ring of *m/z* 239. The MS^3 fragmentation *m/z* 328→*m/z* 203 (Figure S18 B) yielded a series of aromatic, non-chlorinated ions, i.e. *m/z* 159, *m/z* 143 and, upon the scission of terminal CO in *m/z* 143, product ion *m/z* 115.

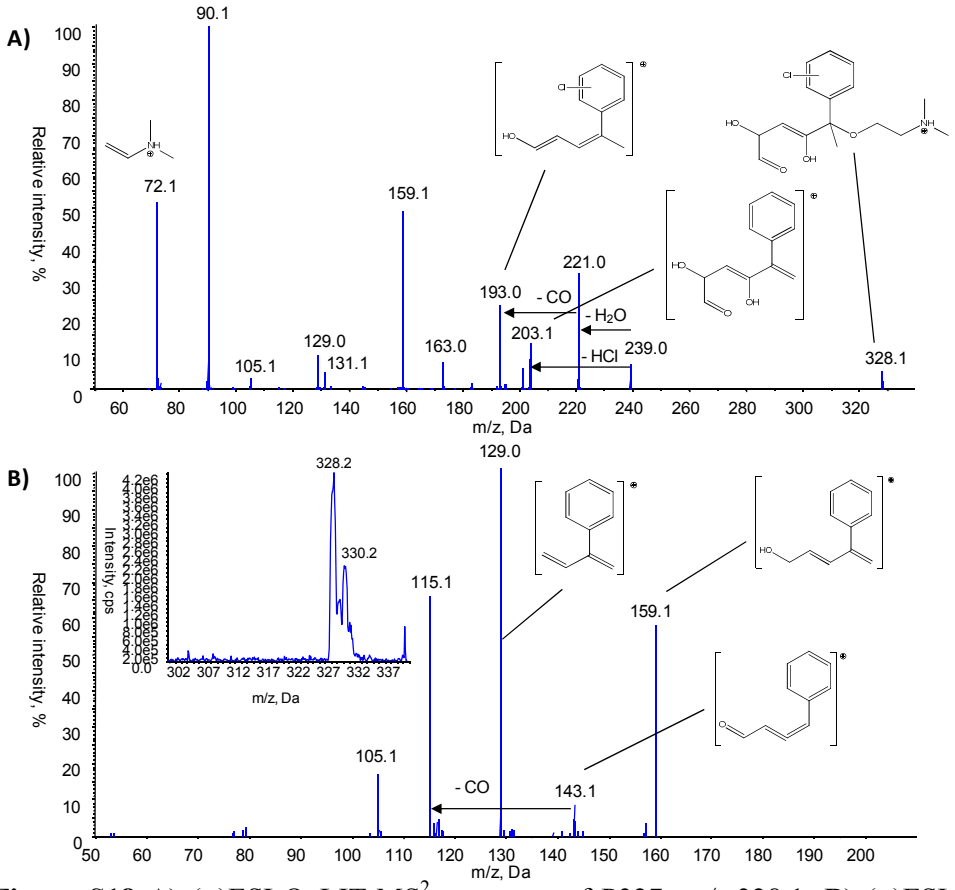

Figure S18 A) (+)ESI-QqLIT-MS^2 spectrum of P327, *m/z* 328.1, **B)** (+)ESI-QqLIT-MS^3 spectrum: *m/z* 328.1→*m/z* 203.1.

P325

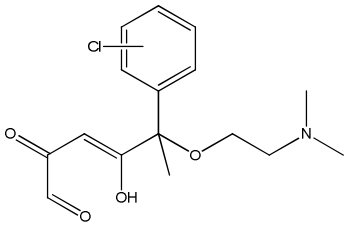

A split peak appearing at t_R=12.9 and 13.0 min was characterized by a monochlorinated mass spectral pattern, with the intensities of molecular ions *m/z* 326 and *m/z* 328 in the ratio 3:1. Based on the obtained spectra, P325 was determined to be a keto-derivative of P327. The shift of -2 Da in the spectrum of *m/z* 326 (Figure S19 A) was in accordance with the substitution of one of the secondary –OH group with the keto-group, as in the case of products P293 and P291. Several fragment ion pairs were noted, differing for 34 Da in the

spectra of P325 and P291, i.e. *m/z* 237/203, *m/z* 219/185, *m/z* 191/157, *m/z* 177/143, and *m/z* 163/129, respectively. Fragmentation of *m/z* 326 also gave rise to aliphatic ions *m/z* 90 and *m/z* 72. Furthermore, sequential fragmentation of *m/z* 326→*m/z* 201 (Figure S19 B) involved the expulsion of HCl form the chlorinated benzene ring and yielded product ions *m/z* 157 and *m/z* 129, previously observed for P291. As in the MS^3 spectrum of *m/z* 292→*m/z* 185, the base peak ion in the MS^3 spectrum of *m/z* 326→*m/z* 201 was fragment ion *m/z* 107. Selection of product ion *m/z* 237 in the MS^3 experiments (Figure S19 C) resulted in the chlorinated aromatic ion *m/z* 219, and, upon the cleavage of terminal CO group ion, *m/z* 191, analogous to ions *m/z* 185 and *m/z* 157 in the spectra of P291.

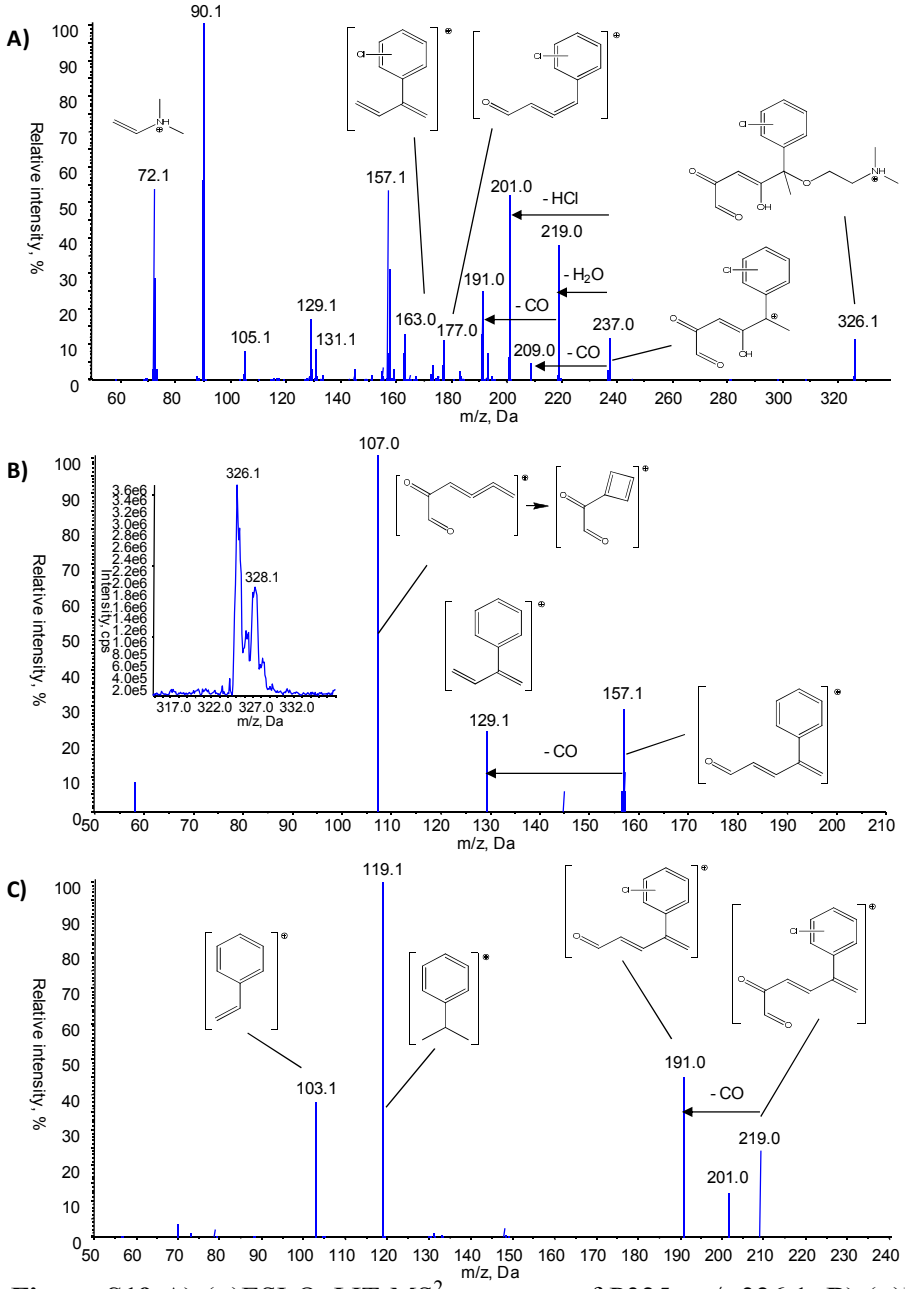

Figure S19 A) (+)ESI-QqLIT-MS^2 spectrum of P325, *m/z* 326.1, **B)** (+)ESI-QqLIT-MS^3 spectrum: *m/z* 326.1→*m/z* 201.1, and **C)** (+)ESI-QqLIT-MS^3 spectrum: *m/z* 326.1→*m/z* 237.0.

P304

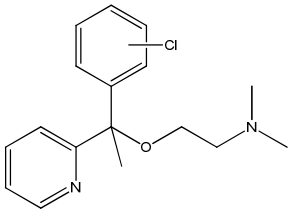

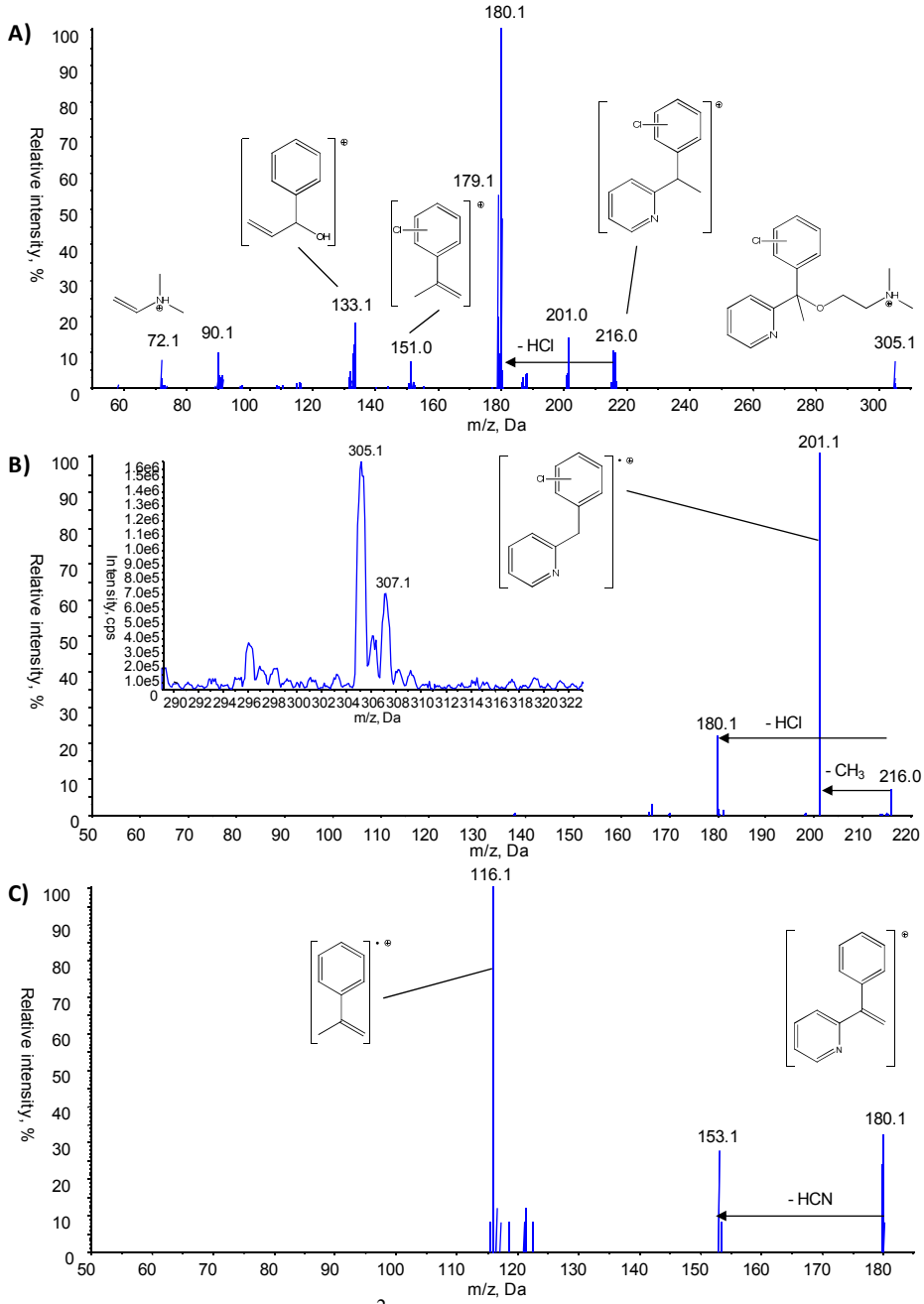

Figure S20 A) (+)ESI-QqLIT-MS^2 spectrum of P304, *m/z* 305.1, **B)** (+)ESI-QqLIT-MS^3 spectrum: *m/z* 305.1→*m/z* 216.1, and **C)** (+)ESI-QqLIT-MS^3 spectrum: *m/z* 305.1→*m/z* 180.1.

The monochlorinated derivative of DOX, product P304 with a molecular ion *m/z* 305 eluted as two peaks at t_R=13.1 and 13.5 min. The mass traces at *m/z* 216 and *m/z* 201 in the MS^2 spectrum of P304 (Figure S20 A) were shifted for +34 Da relative to ions *m/z* 182 and *m/z* 167 in the spectrum of DOX (Figure S4 A), in accordance with the presence of one chlorine substituent. As expected, the unchanged mass of aliphatic ions *m/z* 90 and *m/z* 72 implied that the insertion of chlorine had occurred at benzene or pyridine ring. The formation of a base peak ion *m/z* 180 was rationalized by the expulsion of HCl, characteristic for both chlorinated benzene and pyridine [6]. This assumption was corroborated by the MS^3 sequential fragmentation *m/z* 305→*m/z* 216 (Figure S20 B), and *m/z* 305→*m/z* 180 (Figure S20 C). The spectrum in Figure S20 B also gave rise to product ion *m/z* 201, formed by the scission of a $-CH_3$ moiety. The signal recorded at *m/z* 151 was determined to contain a chlorine atom since in the MS^2 fragmentation of the molecular ion *m/z* 307 this signal was shifted to *m/z* 153 (data not shown). Thus, it was hypothesized that it corresponded to a chlorinated isopropene benzene ion. Favoured chlorination of benzene over pyridine ring is not surprising considering its higher reactivity electrophilic substitution reactions.

P303

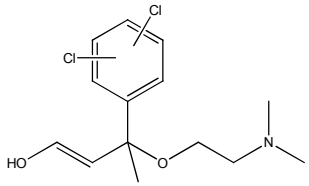

The isotope peak intensity pattern of product P303 with the molecular ions *m/z* 304, *m/z* 306 and *m/z* 308 in the approximate ratio of 1:0.6:0.1, respectively, implied the presence of two chlorine atoms. The MS^2 spectrum of *m/z* 304 (Figure S21 A) contained fragment ions *m/z* 72 and *m/z* 90, diagnostic of an intact backbone of DOX. On the other hand, fragment ions *m/z* 215 and *m/z* 187 were shifted for the mass of two chlorine atoms (i.e. +68 Da) relative to the ions *m/z* 147 and *m/z* 119 observed in the spectra of P235, respectively. The base peak ion *m/z* 179 and product ion *m/z* 151 were derived from the expulsion of one molecule of HCl from the dichlorinated aromatic ring of fragment ions *m/z* 215 and *m/z* 187, respectively [6]. The proposed structures of these fragment ions were confirmed by recording the MS^3 spectrum of *m/z* 215 (Figure S21 B), resulting in product ions *m/z* 179, *m/z* 151 and *m/z* 145, assigned to ions with a dichlorinated benzene ring. The MS^3 spectrum *m/z* 304→*m/z* 151 (Figure S21 C) exhibited a loss of HCl (*m/z* 115) and monochlorinated benzene ion *m/z* 111. Based on the obtained spectra, P303 was determined to be a dichlorinated derivative of P235.

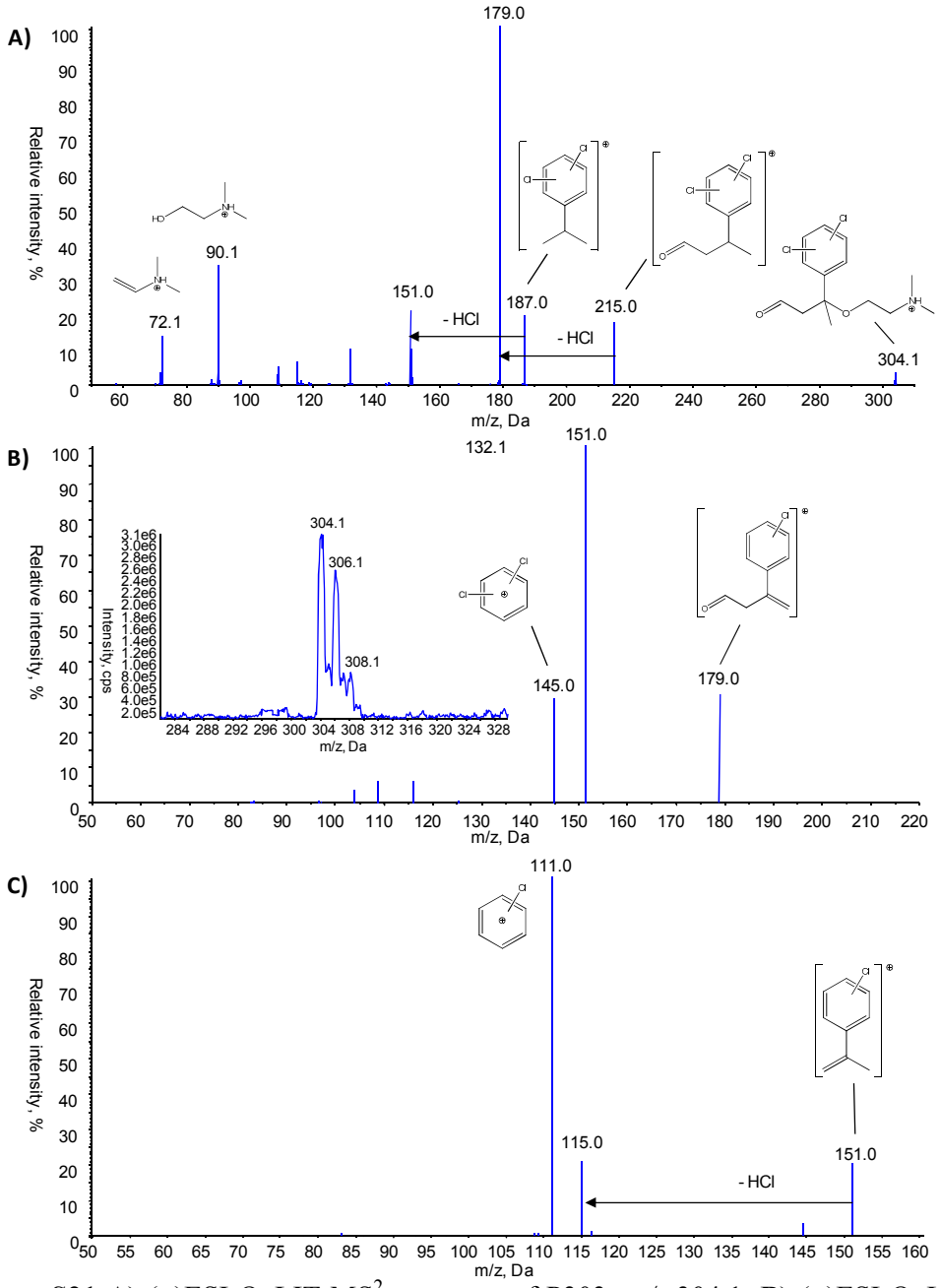

Figure S21 A) (+)ESI-QqLIT-MS^2 spectrum of P303, *m/z* 304.1, **B)** (+)ESI-QqLIT-MS^3 spectrum: *m/z* 304.1→*m/z* 215.0, and **C)** (+)ESI-QqLIT-MS^3 spectrum: *m/z* 304.1→*m/z* 151.0.

Qualitative profiles of the oxidation products of DOX

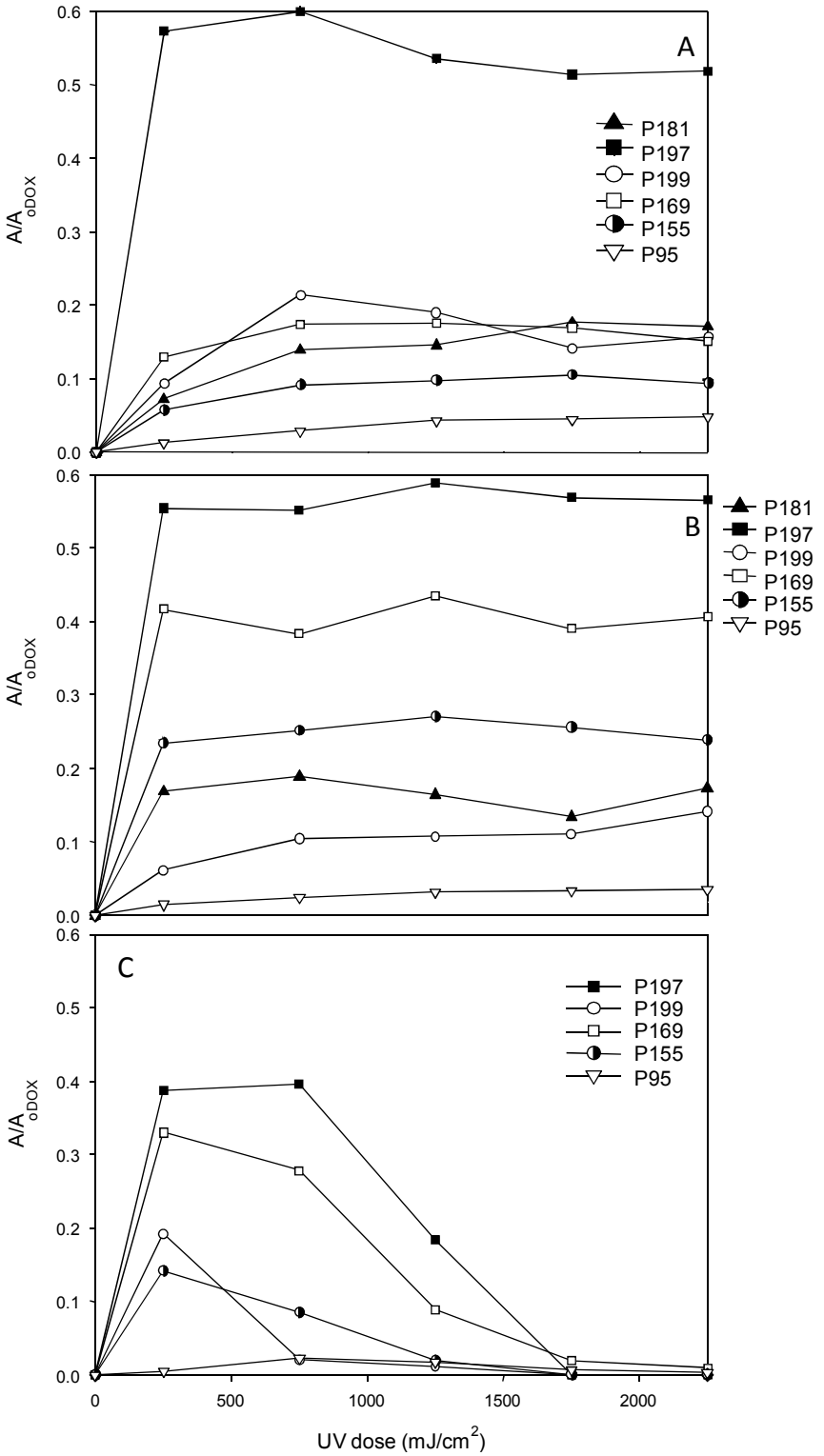

Figure S22 Peak areas of degradation by-products of DOX (P181, P197, P199, P169, P155, P95) formed during **A)** UV, **B)** UV + monochloramine, **C)** UV/H_2O_2 + monochloramine, normalized to the peak area of DOX at t=0 and presented vs UV dose.

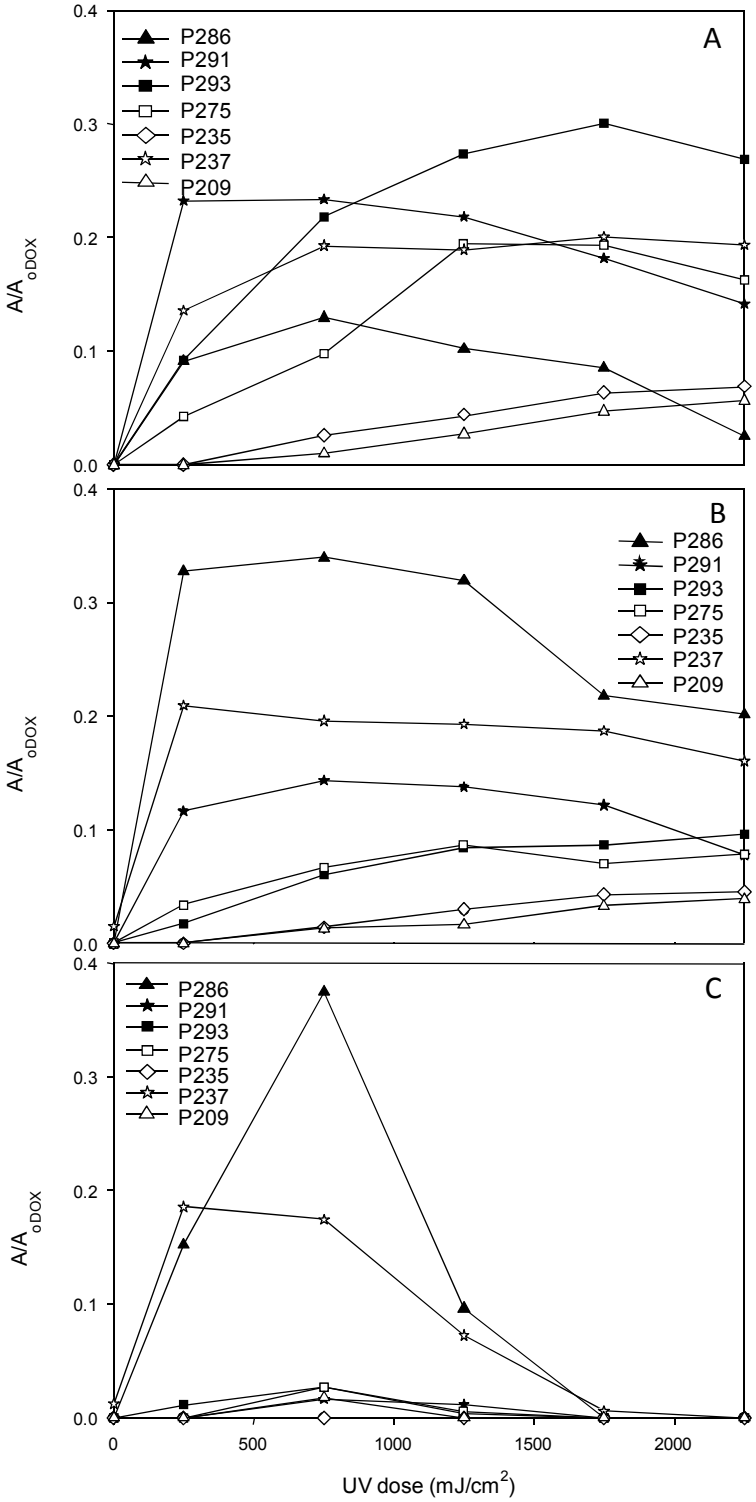

Figure S23 Peak areas of degradation by-products of DOX (P286, P291, P293, P275, P235, P237, 209) formed during A) UV, B) UV + monochloramine, C) UV/H_2O_2 + monochloramine, normalized to the peak area of DOX at t=0 and presented vs UV dose.

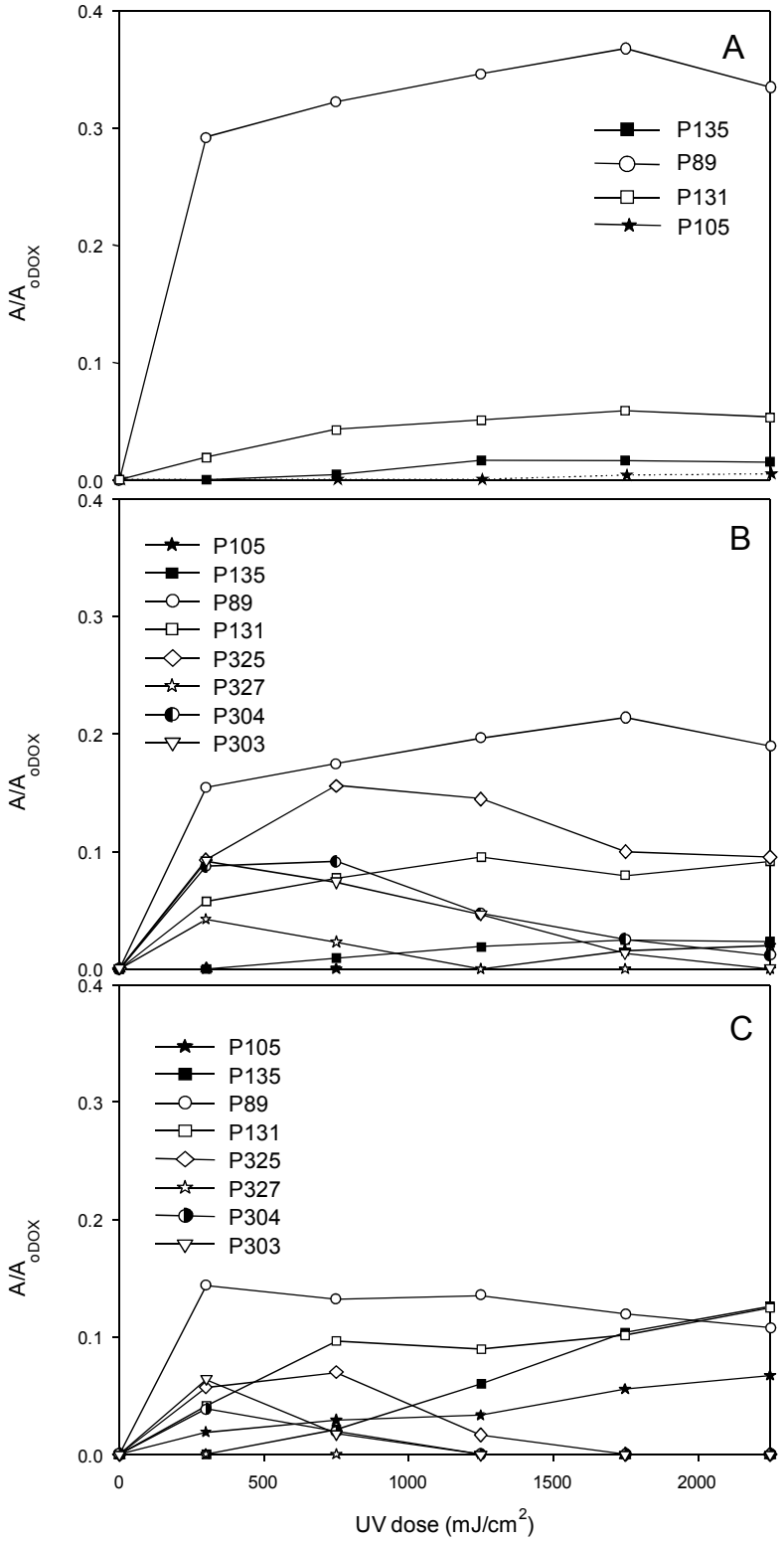

Figure S24 Peak areas of degradation by-products of DOX (P105, P135, P89, P131, P325, P327, P304, P303) formed during A) UV, B) UV + monochloramine, C) UV/H_2O_2 + monochloramine, normalized to the peak area of DOX at t=0 and presented vs UV dose.

References

1. Nogueira, R. F. P.; Oliveira, M. C.; Paterlini, W. C., Simple and fast spectrophotometric determination of H2O 2 in photo-Fenton reactions using metavanadate. *Talanta* **2005,** *66*, (1), 86-91.
2. Bond, T.; Huang, J.; Templeton, M. R.; Graham, N., Occurrence and control of nitrogenous disinfection by-products in drinking water – A review. *Water Research* **2011,** *45*, (15), 4341-4354.
3. Stefan, M. I.; Bolton, J. R., UV direct photolysis of N-nitrosodimethylamine (NDMA): Kinetic and product study. *Helvetica Chimica Acta* **2002,** *85*, (5), 1416-1426.
4. Behan, A., Mass Spectrometry: A Textbook. By Jürgen H. Gross. *PROTEOMICS* **2005,** *5*, (17), 4638-4638.
5. Korfmacher, W. A.; Holder, C. L.; Betowski, L. D.; Mitchum, R. K., Characterization of doxylamine and pyrilamine metabolites via thermospray/mass spectrometry and tandem mass spectrometry. *Biomedical and Environmental Mass Spectrometry* **1988,** *15*, (9), 501-508.
6. McLafferty, F. W.; Turecek, F., *Interpretation of mass spectra*. University Science Books: Sausalito, Calif, 1993.
7. *ChemDraw Ultra 12.0*, 2012.
8. Lambropoulou, D. A.; Hernando, M. D.; Konstantinou, I. K.; Thurman, E. M.; Ferrer, I.; Albanis, T. A.; Fernández-Alba, A. R., Identification of photocatalytic degradation products of bezafibrate in TiO2 aqueous suspensions by liquid and gas chromatography. *Journal of Chromatography A* **2008,** *1183*, (1-2), 38-48.
9. Radjenović, J.; Godehardt, M.; Petrović, M.; Hein, A.; Farré, M.; Jekel, M.; Barceló, D., Evidencing generation of persistent ozonation products of antibiotics roxithromycin and trimethoprim. *Environmental Science and Technology* **2009,** *43*, (17), 6808-6815.
10. Lin, S.-T.; Tien, L.-L.; Kuo, Y.-H.; Shih, K.-S., Mass spectra of 2- and/or 6-alkyl-3-hydroxypyridines. *Organic Mass Spectrometry* **1991,** *26*, (6), 583-586.
11. Tamvakopoulos, C.; Dimas, K.; Sofianos, Z. D.; Hatziantoniou, S.; Han, Z.; Liu, Z. L.; Wyche, J. H.; Pantazis, P., Metabolism and anticancer activity of the curcumin analogue, dimethoxycurcumin. *Clinical Cancer Research* **2007,** *13*, (4), 1269-1277.
12. Oliw, E. H.; Wennman, A.; Hoffmann, I.; Garscha, U.; Hamberg, M.; Jernerén, F., Stereoselective oxidation of regioisomeric octadecenoic acids by fatty acid dioxygenases. *Journal of Lipid Research* **2011,** *52*, (11), 1995-2004.